

## FOR PEER REVIEW - CONFIDENTIAL

### eLife's Review Process

eLife works to improve the process of peer review so that it more effectively conveys the assessment of expert reviewers to authors, readers and other interested parties. In the future we envision a system in which research is first published as a preprint and the outputs of peer review are the primary way research is assessed, rather than journal title.

Our editorial process produces two outputs: i) an assessment by peers designed to be posted alongside a preprint for the benefit of the readers; ii) detailed feedback on the manuscript for the authors, including requests for revisions and suggestions for improvement.

Therefore we want to change how we construct and write peer reviews to make them useful to both authors and readers in a way that better reflects the work you put into reading and thinking about a paper.

eLife reviews now have three parts:

- An **evaluation summary** (in two or three sentences) that captures the major conclusions of the review in a concise manner, accessible to a wide audience.
- A **public review** that details the strengths and weaknesses of the manuscript before you, and discusses whether the authors' claims and conclusions are justified by their data.
- A set of private **recommendations for the authors** that outline how you think the science and its presentation could be strengthened.

All three sections will be used as the basis for an eLife publishing decision, which will, as always, be made after a consultation among the reviewers and editor. Each of the **public reviews** will be published (anonymously) alongside the preprint, together with a response from the authors if they choose. In the case of papers we reject after review, the authors can choose to delay posting until their paper has been published elsewhere.

If this is your first time going through this new process, we ask that you take some time to read our [Reviewer Guide](#), which discusses how we see each section will be used, what it should contain, and what we hope it accomplishes. And we remind you that, with the shift of reviews from private correspondence to public discourse, it is more important than ever that reviews are written in a **clear and constructive manner** appropriate for a public audience and mindful of the impact language choices might have on the authors.

### Information about the manuscript

#### **MKK6 deficiency promotes cardiac dysfunction through MKK3-p38 $\gamma$ / $\delta$ -mTOR hyperactivation**

Tracking no: 03-11-2021-RA-eLife-75250

**Competing interests:** No competing interests declared

#### **Author contributions:**

Rafael Romero-Becerra: Data curation; Formal analysis; Validation; Investigation; Visualization; Methodology; Writing - original draft; Writing - review and editing Alfonso Mora: Data curation; Investigation; Visualization; Methodology; Writing - review and editing Elisa Manieri: Investigation; Methodology Laura Sanz: Investigation; Methodology Ivana Nikolic: Investigation; Methodology Ayelén Santamans: Investigation; Methodology Valle Montalvo-Romeral: Investigation; Methodology Francisco Cruz: Investigation; Methodology; Writing - review and editing Elena Rodríguez: Investigation; Methodology Luis Leiva-Vega: Investigation; Methodology Víctor Bondía: Investigation; Methodology David Filgueiras-Rama: Investigation; Methodology; Writing - review and editing Luis Jiménez-Borreguero: Investigation; Methodology José Jalife: Investigation; Methodology; Writing - review and editing Barbara Gonzalez-Teran: Data curation; Formal analysis; Validation; Investigation; Visualization; Methodology; Writing - original draft; Writing - review and editing Guadalupe Sabio: Conceptualization; Resources; Formal analysis; Supervision; Funding acquisition; Investigation; Visualization; Methodology; Writing - original draft; Project administration; Writing - review and editing

#### **Data Availability:**

All data generated or analysed during this study are included in the manuscript and supporting file; Source Data files have been provided for Figures 1-7

N/A

#### **Ethics:**

Human Subjects: No Animal Subjects: Yes Ethics Statement: This study was performed in strict accordance with the recommendations in the Guide for the Care and Use of Laboratory Animals of the National Institutes of Health. All animal procedures conformed to EU Directive

86/609/EEC and Recommendation 2007/526/EC regarding the protection of animals used for experimental and other scientific purposes, enacted under Spanish law 1201/2005. All of the animals were handled according to approved institutional animal care and use committee protocols (PROEX-215/18) of the Comunidad de Madrid.

bioRxiv preprint doi: <https://doi.org/10.1101/2021.11.15.468612>; this version posted November 16, 2021. The copyright holder for this preprint (which was not certified by peer review) is the author/funder, who has granted bioRxiv a license to display the preprint in perpetuity. It is made available under a [CC-BY 4.0 International license](#).

# 1 **MKK6 deficiency promotes cardiac dysfunction** 2 **through MKK3-p38 $\gamma$ / $\delta$ -mTOR hyperactivation**

3 Rafael Romero-Becerra<sup>1</sup>, Alfonso Mora<sup>1</sup>, Elisa Manieri<sup>1</sup>, Laura Sanz<sup>1</sup>, Ivana Nikolic<sup>1</sup>,  
4 Ayelén M. Santamans<sup>1</sup>, Valle Montalvo-Romeral<sup>1</sup>, Francisco Miguel Cruz Uréndez<sup>1</sup>,  
5 Maria Elena Rodríguez<sup>1</sup>, Luis Leiva-Vega<sup>1</sup>, Víctor Bondía<sup>1</sup>, David Filgueiras-Rama<sup>1,2,3</sup>,  
6 Luis Jesús Jiménez-Borreguero<sup>1</sup>, José Jalife<sup>1,2,4</sup>, Bárbara González-Terán<sup>1,5#</sup> &  
7 Guadalupe Sabio<sup>1#</sup>

8

9 <sup>1</sup>Centro Nacional de Investigaciones Cardiovasculares (CNIC), Madrid, Spain.

10 <sup>2</sup>CIBER de Enfermedades Cardiovasculares (CIBERCV), Madrid, Spain

11 <sup>3</sup>Hospital Clínico Universitario San Carlos, Madrid, Spain.

12 <sup>4</sup>Center for Arrhythmia Research, Department of Internal Medicine, University of Michigan,  
13 Ann Arbor, MI, USA

14 <sup>5</sup>Gladstone Institutes, San Francisco, CA, USA.

15

16

17 Keywords: aging/cardiac hypertrophy/MKK3/MKK6/mTOR/p38 MAPK

18

19 # Address correspondence to:

20 Guadalupe Sabio & Bárbara González-Terán

21 Centro Nacional de Investigaciones Cardiovasculares (CNIC).

22 Calle de Melchor Fernández Almagro, 3, 28029, Madrid, Spain.

23 [gsabio@cnic.es](mailto:gsabio@cnic.es)

24 [barbara.gonzalezteran@gladstone.ucsf.edu](mailto:barbara.gonzalezteran@gladstone.ucsf.edu)

25

bioRxiv preprint doi: <https://doi.org/10.1101/2021.11.15.468612>; this version posted November 16, 2021. The copyright holder for this preprint (which was not certified by peer review) is the author/funder, who has granted bioRxiv a license to display the preprint in perpetuity. It is made available under a [CC-BY 4.0 International license](#).

26

27 **ABSTRACT**

28

29 Stress-activated p38 kinases control a plethora of functions and their dysregulation has

30 been linked to development of steatosis, obesity, immune disorders and cancer.

31 Therefore, they have been identified as potential targets for novel therapeutic strategies.

32 There are four p38 family members (p38 $\alpha$ , p38 $\beta$ , p38 $\gamma$ , and p38 $\delta$ ) that are activated by

33 MKK3 and MKK6. Here we demonstrate that lack of MKK6 reduces the life span in

34 mice. Longitudinal study of cardiac function in *Mkk6*<sup>-/-</sup> mice showed that young mice

35 have cardiac hypertrophy which progresses to cardiac dilatation and fibrosis with age.

36 Mechanistically, lack of MKK6 blunts p38 $\alpha$  activation while causing MKK3-p38 $\gamma/\delta$ 

37 hyperphosphorylation and increased mTOR signaling, resulting in cardiac hypertrophy.

38 Cardiac hypertrophy in *Mkk6*<sup>-/-</sup> mice is reverted by knocking out either p38 $\gamma$  or p38 $\delta$ , or

39 by inhibiting mTOR pathway with rapamycin. In conclusion, we have identified a key

40 role for the MKK3/6-p38 $\gamma/\delta$  pathway in the development of cardiac hypertrophy, which41 has important implications for the clinical use of p38 $\alpha$  inhibitors in the long-term

42 treatment since they might result in cardiotoxicity.

43

## 44 INTRODUCTION

45 Cardiac hypertrophy is an adaptive response of the heart to hemodynamic stress  
46 that can be physiologic (e.g., pregnancy or exercise) or pathological (e.g., hypertension  
47 or valvular disease). Physiological cardiac hypertrophy is accompanied with a normal or  
48 even enhanced cardiac function, while pathological forms of hypertrophy are  
49 accompanied by myocardial dysfunction and fibrosis and represent a risk factor for  
50 ventricular arrhythmias and sudden cardiac death (Maillet *et al*, 2013; Nakamura &  
51 Sadoshima, 2018; Oldfield *et al*, 2020).

52 Initially, cardiac hypertrophy is induced as a compensatory response to preserve  
53 cardiac function under stressful conditions, a process known as adaptive cardiac  
54 hypertrophy. However, if the pathological stimulus is maintained, this adaptive cardiac  
55 hypertrophy will eventually lead to the development of pathological cardiac  
56 hypertrophy and heart failure (Nakamura & Sadoshima, 2018; Oldfield *et al.*, 2020).  
57 The form of cardiac hypertrophy developed will depend on the type of the hypertrophic  
58 stimuli, the duration of the stimuli and the downstream signaling involved (Nakamura  
59 & Sadoshima, 2018; Oldfield *et al.*, 2020; Shimizu & Minamino, 2016). Several  
60 signalling pathways known to promote physiological cardiac hypertrophic growth,  
61 when persistently activated have been found to drive pathological hypertrophy and  
62 cardiac dysfunction (Heineke & Molkentin, 2006; Maillet *et al.*, 2013; Nakamura &  
63 Sadoshima, 2018; Porrello *et al*, 2008). For instance, IGF1 or Akt transgenic mice  
64 develop proportionately enlarged hearts with initially normal cardiac function, which  
65 over time progress to pathological hypertrophy with impaired cardiac function  
66 (DeLaughter *et al*, 1999; Shiojima *et al*, 2005).

67 Stress-inducing stimuli in the heart activate several mitogen-activated protein  
68 kinases (MAPKs) including the p38 family. p38 kinases control a wide range of

bioRxiv preprint doi: <https://doi.org/10.1101/2021.11.15.468612>; this version posted November 16, 2021. The copyright holder for this preprint (which was not certified by peer review) is the author/funder, who has granted bioRxiv a license to display the preprint in perpetuity. It is made available under aCC-BY 4.0 International license.

69 processes and their dysregulation has been linked to numerous diseases, making them a  
70 promising pharmacological target for therapeutic use (Canovas & Nebreda, 2021). This  
71 family consists of four isoforms:  $\alpha$ ,  $\beta$ ,  $\gamma$ , and  $\delta$ , with p38 $\alpha$  having been the most broadly  
72 studied, whereas knowledge of the other p38 isoforms has been limited by a reduced  
73 availability of isoform-specific reagents. Our previous work showed that p38 $\gamma$  and p38 $\delta$   
74 are expressed in the heart and participate in the cardiac hypertrophic response. We have  
75 shown that p38 $\gamma/\delta$  mediate early postnatal cardiac hypertrophy by promoting mTOR-  
76 induced cell growth (Gonzalez-Teran *et al*, 2016).

77 An essential feature of both physiological and pathological hypertrophy is  
78 increased protein synthesis, critically regulated by the mammalian target of rapamycin  
79 (mTOR) pathway mainly through the phosphorylation of its downstream substrates.  
80 Activation of mTOR signaling is increased during postnatal cardiac development  
81 (Gonzalez-Teran *et al.*, 2016) as well as in the hearts of transgenic mouse models  
82 suffering from physiological cardiac hypertrophy (McMullen *et al*, 2004a; McMullen *et al*,  
83 2004b; Shioi *et al*, 2000; Shioi *et al*, 2003). Moreover, the specific mTOR inhibitor  
84 rapamycin attenuates and reverses cardiac-overload-induced pathological hypertrophy  
85 (Shioi *et al.*, 2003). Conversely, mTOR pathway activation mediated by p38 $\gamma$  and p38 $\delta$   
86 MAPKs has been implicated in the control of postnatal cardiac hypertrophic growth and  
87 angiotensin-II-induced cardiac hypertrophy (Gonzalez-Teran *et al.*, 2016).

88 Here, we demonstrate that in the heart MKK3 activates p38 $\gamma/\delta$ , whereas  
89 MKK6 activates p38 $\alpha$ . Furthermore, we find that *Mkk6*<sup>-/-</sup> mice exhibit cardiac  
90 hypertrophy caused by hyperactivation of the MKK3-p38 $\gamma/\delta$  axis, which progresses to a  
91 pathological cardiac hypertrophy phenotype with age. Our results have important  
92 implications for the clinical use of p38 $\alpha$  inhibitors in the long-term treatment since they  
93 might result in cardiotoxicity.

## 94 RESULTS

### 95 MKK6-deficient mice die prematurely

96 Several studies have addressed the role of p38 signaling in homeostasis and  
97 disease (Nikolic *et al*, 2020; Romero-Becerra *et al*, 2020). While mice lacking both  
98 MKK3 and MKK6 die in mid-gestation with mutant embryos demonstrating  
99 abnormalities of the placenta and embryonic vasculature (Brancho *et al*, 2003), mice  
100 individually lacking MKK3 or MKK6 are viable and fertile, suggesting partial  
101 functional redundancy (Lu *et al*, 1999; Tanaka *et al*, 2002; Wysk *et al*, 1999). However,  
102 the role of the p38 pathway in aging remains incompletely understood. Therefore, we  
103 examined mice harboring germline deletion of *Mkk6* (*Mkk6*<sup>-/-</sup>) (Tanaka *et al.*, 2002) at  
104 advanced age. Mice lacking *MKK6* have reduced body weight compared to age-  
105 matched wild type (WT) animals (Figure 1A, B), which can be partially explained by a  
106 dramatic reduction in white adipose tissue (Figure 1C). This agrees with previous  
107 studies demonstrating that *Mkk6*<sup>-/-</sup> mice are protected against diet-induced obesity with  
108 increase browning of the epididymal white adipose tissue (eWAT) (Matesanz *et al*,  
109 2017).

110 Additionally, these mice exhibit an abnormal posture characterized by a hunched  
111 position and the development of thoracic kyphosis and severe ataxia (Figure 1D and  
112 Figure 1 – video supplement 1). As a consequence of all these phenotypic alterations,  
113 *Mkk6*<sup>-/-</sup> mice suffer premature death, the first mice dying at 51 weeks of age with a  
114 median life span of 76 weeks (Figure 1E).

115

### 116 MKK6-deficient mice develop increased age-related cardiac dysfunction

117 The downstream kinases of MKK6 have been implicated in  
118 major cardiovascular abnormalities during development. Combined deletion of p38 $\alpha$

bioRxiv preprint doi: <https://doi.org/10.1101/2021.11.15.468612>; this version posted November 16, 2021. The copyright holder for this preprint (which was not certified by peer review) is the author/funder, who has granted bioRxiv a license to display the preprint in perpetuity. It is made available under a [CC-BY 4.0 International license](#).

119 and p38 $\beta$  results in cardiac defects during embryonic development (del Barco Barrantes  
120 *et al.*, 2011), whereas p38 $\gamma/\delta$  deficient mice exhibit reduced cardiomyocyte  
121 hypertrophic growth and smaller hearts (Gonzalez-Teran *et al.*, 2016). This prompted us  
122 to speculate that cardiac abnormalities could be one of the underlying causes of  
123 premature death of *Mkk6*<sup>-/-</sup> mice. Echocardiographic analyses of 12 to 14-month-old  
124 mice demonstrated eccentric hypertrophy in *Mkk6*<sup>-/-</sup> mice compared to control mice, as  
125 detected by thinning of the left ventricle (LV) wall, as well as increased left ventricular  
126 internal diameter (LVID) and left ventricular volume, especially during the systole  
127 (Figure 2A). Cardiac enlargement compromised systolic function, evidenced by a  
128 decreased in the ejection fraction and fractional shortening. However, the diastolic  
129 function appeared to be maintained, with a normal E/A wave velocities ratio and  
130 isovolumetric relaxation time (Figure 2B). Moreover, *Mkk6*<sup>-/-</sup> mice exhibit bradycardia  
131 (Figure 2C). We performed picosirius red staining for collagen and quantified positive  
132 areas in serial histologic sections from *Mkk6*<sup>-/-</sup> and WT hearts and found cardiac fibrotic  
133 lesions in *Mkk6*<sup>-/-</sup> old mice (Figure 2D). To discard hypertension as a possible  
134 contributor of the cardiac dysfunction we evaluated blood pressure in these animals.  
135 *Mkk6*<sup>-/-</sup> mice did not present differences in blood pressure compared to age-matched  
136 controls (Figure 2E).

137

### 138 **Young MKK6-deficient mice present cardiac hypertrophy**

139 Cardiac dysfunction may result from an initial compensated cardiac hypertrophy  
140 that with time becomes pathological (Nakamura & Sadoshima, 2018).  
141 Echocardiographic analysis at 9 weeks of age demonstrated cardiac hypertrophy in  
142 MKK6-deficient animals when compared with controls, as detected by measures of left  
143 ventricular mass, interventricular septal thickness, left ventricular posterior wall

bioRxiv preprint doi: <https://doi.org/10.1101/2021.11.15.468612>; this version posted November 16, 2021. The copyright holder for this preprint (which was not certified by peer review) is the author/funder, who has granted bioRxiv a license to display the preprint in perpetuity. It is made available under aCC-BY 4.0 International license.

144 thickness, and left ventricular internal diameter (Figure 3A). However, cardiac  
145 enlargement did not compromise systolic function or diastolic function (given by the  
146 ejection fraction and the E/A wave velocity ratio, respectively) but was accompanied by  
147 increases in stroke volume and cardiac output (Figure 3B). Gross anatomic and  
148 histologic analyses confirmed these non-invasive findings as MKK6-deficient hearts  
149 were larger than WT controls when normalized to tibia length (TL) (Figure 3C&D), a  
150 difference that was not apparent at 4 weeks of age. Serial analysis of heart weight  
151 (HW)/TL over 15 weeks demonstrated enhanced cardiac growth in *Mkk6*<sup>-/-</sup> mice (Figure  
152 3D). The progressive increase in size of *Mkk6*<sup>-/-</sup> hearts correlated with increased  
153 cardiomyocyte cross-sectional area, consistent with enhanced hypertrophic growth  
154 (Figure 3E). Hypertension was excluded as a possible contributor to this increased  
155 growth as *Mkk6*<sup>-/-</sup> mice demonstrate reduced systolic blood pressures when compared to  
156 age-matched controls (Figure 3 – figure supplement 1A). Fibrosis and reactivation of a  
157 “fetal gene program” (e.g., *Nppa*, *Nppb*, *Acta2*, *Myh7*) are hallmark features of  
158 pathologic hypertrophy (Bernardo *et al*, 2010). Histological cardiac examination  
159 revealed no evidence of fibrosis in *Mkk6*<sup>-/-</sup> heart sections (Figure 3 – figure supplement  
160 1B). We also found no difference in the expression of fibrotic genes including *Colla1*,  
161 *Col3a1*, and  *or markers of the fetal gene program (Figure 3 – figure supplement 1C,  
162 D). No meaningful changes were visible for *Nppa* or *Nppb* (Figure 3 – figure  
163 supplement 1D). These observations suggest that at 9 weeks of age *Mkk6*<sup>-/-</sup> hearts show  
164 a non-pathological cardiac hypertrophy.*

165 To confirm the MKK6 autonomous effect in cardiomyocytes we employed a  
166 murine conditional MKK6 allele (*Mkk6*<sup>LoxP</sup>)<sup>23</sup> and two cardiomyocyte Cre-expressing  
167 lines (*MCK-Cre* (Bruning *et al*, 1998) and *αMHC-Cre* (McFadden *et al*, 2005)) to  
168 assess the consequences of MKK6 genetic ablation in postnatal cardiomyocytes. MCK-

bioRxiv preprint doi: <https://doi.org/10.1101/2021.11.15.468612>; this version posted November 16, 2021. The copyright holder for this preprint (which was not certified by peer review) is the author/funder, who has granted bioRxiv a license to display the preprint in perpetuity. It is made available under aCC-BY 4.0 International license.

169 Cre is active in striated muscle, and the *MCK-Cre*, *Mkk6<sup>LoxP/LoxP</sup>* (*Mkk6<sup>MCK-KO</sup>*) mice  
 170 demonstrated specific and efficient deletion of MKK6 in the heart and skeletal muscle  
 171 tissues, but not in spleen or liver (Figure 4 – figure supplement 1A, B). Importantly, the  
 172 cardiac phenotype of 9-weeks-old *Mkk6<sup>MCK-KO</sup>* mice resembled that of *Mkk6<sup>-/-</sup>* animals  
 173 (Figure 4A-C). Similar results were obtained with  *$\alpha$ MHC-Cre*, *Mkk6<sup>LoxP/LoxP</sup>*  
 174 (*Mkk6 <sup>$\alpha$ MHC-KO</sup>*) mice (Figure 4D-F). These data collectively confirm that  
 175 cardiomyocyte MKK6 controls heart growth.

176

### 177 **MKK6-deficient hearts have increased MKK3-p38 $\gamma$ / $\delta$ activation**

178 MKK6 is a critical upstream activator of p38 MAPKs, but its specificity for  
 179 individual p38 family isoforms is not well established. We assessed the relative levels  
 180 of phosphorylated p38 isoforms by immunoprecipitation in *Mkk6<sup>-/-</sup>* hearts, which  
 181 demonstrated hyperphosphorylation of p38 $\gamma$  and p38 $\delta$  (Figure 5A) with a simultaneous  
 182 reduction in phosphorylation of p38 $\alpha$  (Figure 5B). Immunoblot analysis also revealed  
 183 increased levels of phosphorylated MKK3, the other main p38 upstream activator, in  
 184 *Mkk6<sup>-/-</sup>* hearts (Figure 5C). This observation suggested that increased phosphorylation  
 185 of p38 $\gamma$  and p38 $\delta$  in the *Mkk6<sup>-/-</sup>* hearts resulted from MKK3 activation. Accordingly,  
 186 phosphorylation of p38 $\gamma$  and p38 $\delta$  was strongly reduced in MKK3-deficient mice,  
 187 whereas p38 $\alpha$  phosphorylation was not changed appreciably (Figure 5D). In addition,  
 188 hearts of *Mkk3<sup>-/-</sup>* mice were smaller at 9 weeks of age when compared with age-matched  
 189 WT controls (Figure 5E), a finding consistent with the previously described roles of  
 190 p38 $\gamma$  and p38 $\delta$  in promoting postnatal cardiac hypertrophic growth (Gonzalez-Teran *et*  
 191 *al.*, 2016). Taken together, these observations indicate that MKK6 primarily targets  
 192 p38 $\alpha$  and MKK3 p38 $\gamma$  and p38 $\delta$ . In addition, they suggest that the MKK6 deficiency  
 193 leads to cardiac hypertrophy via activation of MKK3 and p38 $\gamma$  and p38 $\delta$ .

## 195 **Hypertrophy in MKK6-deficient hearts is mediated by p38 $\gamma/\delta$**

196 To confirm that enhanced hypertrophic growth in MKK6-deficient mice is  
197 mediated by modulation of p38 $\gamma/\delta$  activation, we introduced a deletion of p38 $\gamma$  in the  
198 context of MKK6 deficiency. The double mutant combination (*Mkk6*<sup>-/-</sup>; p38 $\gamma$ <sup>-/-</sup>) rescued  
199 normal cardiac growth, as the heart sizes and cardiomyocyte cross-sectional areas of the  
200 double-mutants were equivalent to those of WT controls (Figure 6A-C). We further  
201 demonstrated the requirement for p38 $\delta$  to be cell-autonomous in striated muscle using a  
202 p38 $\delta$  conditional allele (*Mapk13*<sup>LoxP</sup>). MKK6-deficient hearts lacking p38 $\delta$  in their  
203 myocytes (*Mkk6*<sup>-/-</sup>; *MCK-Cre*; p38 $\delta$ <sup>LoxP/LoxP</sup> hearts) were similar in size to those of mice  
204 lacking p38 $\delta$  in their myocytes (*MCK-Cre*; p38 $\delta$ <sup>LoxP/LoxP</sup> (p38 $\delta$ <sup>MCK-KO</sup>)), with no  
205 appreciable increase in cardiomyocyte cross-sectional area (Figure 6D-F). Collectively,  
206 these data demonstrate that enhanced cardiac hypertrophic growth in MKK6-deficient  
207 mice is mediated by hyperactivation p38 $\gamma/\delta$  of signaling in striated muscle.

208

## 209 **mTOR pathway hyperactivation mediated hypertrophy in MKK6-deficient hearts**

210 The p38 $\gamma$  and p38 $\delta$  isoforms have previously been demonstrated to promote  
211 cardiac hypertrophic growth through activation of mTOR signaling (Gonzalez-Teran *et*  
212 *al.*, 2016). As expected from that finding, immunoblot analysis of *Mkk6*<sup>-/-</sup> mouse hearts  
213 showed an increase in mTOR pathway activation (Figure 7A). As protein synthesis  
214 represents a key target of the mTOR signaling pathway and is critical for cardiomyocyte  
215 hypertrophic growth, we assessed eukaryotic initiation/elongation factors by  
216 immunoblot analyses. We found an overall increase in translational activation in *Mkk6*<sup>-/-</sup>  
217 hearts relative to WT (Figure 7B). We corroborated these findings by analyzing  
218 puromycin incorporation into newly synthesized peptides in WT and *Mkk6*<sup>-/-</sup> hearts,

bioRxiv preprint doi: <https://doi.org/10.1101/2021.11.15.468612>; this version posted November 16, 2021. The copyright holder for this preprint (which was not certified by peer review) is the author/funder, who has granted bioRxiv a license to display the preprint in perpetuity. It is made available under aCC-BY 4.0 International license.

219 which demonstrated greater puromycin-labeling (Figure 7C) and overall protein content  
220 (Figure 7D) in mutant hearts.

221 We next examined the extent to which cardiac hypertrophy in *Mkk6*<sup>-/-</sup> mice is  
222 mediated by increased mTOR signaling. We blocked mTOR activation by daily  
223 intraperitoneal injection of rapamycin, a potent and specific small molecule mTOR  
224 inhibitor, from 3 to 9 weeks of age. This treatment was sufficient to bring the heart size  
225 (HW/TL) of *Mkk6*<sup>-/-</sup> animals close to that of WT age-matched controls, which  
226 corresponded with a robust reduction in cardiomyocyte cross-sectional area in *Mkk6*<sup>-/-</sup>  
227 mice (Figure 4), altogether suggesting that the cardiac hypertrophy in *Mkk6*<sup>-/-</sup> mice  
228 results from hyperactivation of mTOR signaling.

229

## 230 **DISCUSSION**

231 The present study provides several independent lines of evidence supporting a  
232 critical role for the MKK3/6–p38 $\gamma/\delta$  signaling pathway in the development of cardiac  
233 hypertrophy. The hypertrophy developed seems to be physiological in young animals,  
234 with normal or even increased cardiac function at baseline. However, aging induced the  
235 development of cardiac dysfunction and premature death. Extensive analysis with  
236 different knockout mouse models shows that in the absence of MKK6, the MKK3-  
237 stimulated p38 $\gamma/\delta$  kinases become hyperactivated and induce enhanced postnatal  
238 hypertrophic growth through the mTOR pathway. Our results also confirm that the two  
239 main up-stream p38 activators are strongly biased toward the activation of specific p38  
240 MAPK isoforms in the heart, with p38 $\gamma/\delta$  mainly regulated by MKK3 and p38 $\alpha$  by  
241 MKK6, at least in homeostatic conditions.

242 Previous work has implicated multiple p38 isoforms in disease models of  
243 pathologic hypertrophy (Nikolic *et al.*, 2020; Romero-Becerra *et al.*, 2020), whereas

bioRxiv preprint doi: <https://doi.org/10.1101/2021.11.15.468612>; this version posted November 16, 2021. The copyright holder for this preprint (which was not certified by peer review) is the author/funder, who has granted bioRxiv a license to display the preprint in perpetuity. It is made available under aCC-BY 4.0 International license.

244 p38 $\gamma$  and p38 $\delta$  isoforms appeared to be involved primarily in regulating postnatal  
245 physiological cardiac growth and the metabolic switch during cardiac early postnatal  
246 development (Gonzalez-Teran *et al.*, 2016). Such reports, however, have not addressed  
247 how different p38 MAPK isoforms are regulated and the relative contributions of  
248 MKK3 and MKK6 to cardiac hypertrophic phenotypes have so far remained unclear.  
249 Indeed, either overexpression of constitutively active or dominant negative forms of  
250 MKK3/6 *in vitro* yields cardiac hypertrophy (Braz *et al.*, 2003; Streicher *et al.*, 2010;  
251 Zechner *et al.*, 1997). Our *in vivo* data support a model wherein MKK3 activity  
252 promotes hypertrophic growth. We show that MKK3 hyperactivation resulting from  
253 MKK6 deletion leads to cardiac hypertrophy while MKK3 genetic ablation results in  
254 reduced postnatal cardiac growth. We also demonstrate that deficiency of MKK6 in  
255 cardiomyocytes is sufficient to result in cardiac hypertrophy, attributable to both,  
256 MKK6 direct function in inducing hypertrophy via p38-mediated signaling as well as its  
257 role as a negative regulator of MKK3 activity. This negative regulation may be a direct  
258 action of MKK6 or may be mediated by p38 $\alpha$ , whose phosphorylation levels are  
259 strongly decreased in *Mkk6*<sup>-/-</sup> hearts. The last possibility is further supported by evidence  
260 indicating that p38 $\alpha$  might negatively regulate the MKK3/6 upstream kinase MAP3K  
261 TAK1 (Singhirunusorn *et al.*, 2005). Indeed, we have found that in other tissues, lack  
262 of p38 $\alpha$  induces p38 $\gamma$  and p38 $\delta$  activation (Matesanz *et al.*, 2018). The negative  
263 feedback activity of p38 $\alpha$  is consistent with MKK3 hyperphosphorylation identified in  
264 *Mkk6*<sup>-/-</sup> mice. Our results provide the first demonstration that MKK3 preferentially  
265 regulates p38 $\gamma$  and p38 $\delta$  activation, whereas MKK6 is responsible for p38 $\alpha$  regulation.  
266 MKK6-deficient mice show p38 $\gamma/\delta$  hyperactivation and impaired p38 $\alpha$   
267 activation, possibly implicating any of these isoforms in the observed phenotypes.  
268 Through the use of multiple *in vivo* models, we show that hyperphosphorylated MKK3

bioRxiv preprint doi: <https://doi.org/10.1101/2021.11.15.468612>; this version posted November 16, 2021. The copyright holder for this preprint (which was not certified by peer review) is the author/funder, who has granted bioRxiv a license to display the preprint in perpetuity. It is made available under aCC-BY 4.0 International license.

269 promotes cardiac hypertrophic growth through activation of p38 $\gamma$ - and p38 $\delta$ -mediated  
270 mTOR signaling in the heart. This is consistent with our earlier work showing an  
271 essential role for these p38 isoforms in mTOR-dependent of physiologic and  
272 pathological cardiac hypertrophy (Gonzalez-Teran *et al.*, 2016), as well as with  
273 previous reports indicating that p38 $\alpha$  does not mediate hypertrophic responses in animal  
274 models of pressure-overload cardiac hypertrophy (Nishida *et al.*, 2004). This conclusion  
275 is corroborated by the reversion of cardiac hypertrophy in MKK6-deficient mice also  
276 deficient for cardiac p38 $\gamma$  or p38 $\delta$ , and further corroboration comes from the ability of  
277 the mTOR inhibitor rapamycin to prevent cardiac hypertrophy during early postnatal  
278 cardiac development in MKK6-deficient mice. These findings correlate with impaired  
279 p38 $\gamma$  and p38 $\delta$  activation and reduced postnatal hypertrophic growth in MKK3-deficient  
280 mice.

281 The p38 $\gamma$ - and p38 $\delta$ -mediated control of cardiac hypertrophy during postnatal  
282 cardiac development resides in cardiomyocytes (Gonzalez-Teran *et al.*, 2016).  
283 Accordingly, lack of MKK6 in skeletal muscle or cardiomyocytes yields the same  
284 phenotype as global MKK6 deficiency. Furthermore, the blockade of cardiac  
285 hypertrophy in MKK6-deficient mice upon deletion of p38 $\delta$  specifically in striated  
286 muscle indicates that cardiac p38 $\delta$  lies downstream of MKK6 in the signaling pathway  
287 controlling hypertrophic growth. Interestingly, reversion of the MKK6-deficient  
288 phenotype upon p38 $\delta$  deletion was greater than that achieved upon deletion of p38 $\gamma$   
289 (Figure 6), consistent with the reported dominance of p38 $\delta$  in regulating cardiac  
290 hypertrophic growth (Gonzalez-Teran *et al.*, 2016).

291 Young MKK6-deficient mice develop a cardiac hypertrophy that could be  
292 classified as physiological, characterized by a proportionate increase in heart size with  
293 maintenance of a normal cardiac structure. Moreover, cardiac function was normal, with

bioRxiv preprint doi: <https://doi.org/10.1101/2021.11.15.468612>; this version posted November 16, 2021. The copyright holder for this preprint (which was not certified by peer review) is the author/funder, who has granted bioRxiv a license to display the preprint in perpetuity. It is made available under a [CC-BY 4.0 International license](#).

294 increased cardiac output and stroke volume, and there was no evidence of fibrosis nor  
295 re-expression of the cardiac stress fetal gene program. Physiologic cardiac hypertrophy  
296 is an adaptive response that increases ventricular mass while maintaining or enhancing  
297 cardiac function (Kang, 2006; Nakamura & Sadoshima, 2018). However, it has  
298 increasingly become appreciated that sustained activation of the pathways that drive this  
299 beneficial response can ultimately result in pathological remodeling and associated  
300 sudden cardiac death (Condorelli *et al*, 2002; Lauschke & Maisch, 2009; Matsui *et al*,  
301 2002; McMullen *et al.*, 2004a; Oldfield *et al.*, 2020; Shioi *et al*, 2002). In agreement  
302 with this, the cardiac hypertrophy observed in *Mkk6*<sup>-/-</sup> mice becomes deleterious with  
303 age, compromising the cardiac function and likely contributing to the reduced survival  
304 observed in these mice. Our results identify a key role for the MKK3/6-p38 $\gamma/\delta$  pathway  
305 in the development of cardiac hypertrophy and illustrates how, depending on the  
306 stimulus, the activation of the same pathway can promote the progression from a  
307 physiological to a pathological phenotype.

308         The activation of p38 $\alpha$  pathway has been linked to several diseases, suggesting  
309 that this pathway could represent a target for their treatment. However, the results from  
310 the clinical trials have been disappointing so far (Canovas & Nebreda, 2021). p38 $\alpha$   
311 inhibitors have been the more profoundly studied. However, these studies usually do not  
312 consider the possible undesired effect of p38 $\alpha$  inhibition upon the other p38 pathway  
313 kinases, which could be among the reasons of failure in the outcomes. Our results show  
314 an example of how p38 $\alpha$  inhibition leads to an unexpected activation of MKK3-p38 $\gamma/\delta$ ,  
315 having deleterious effects in the heart in the long-term. Our finding suggests that  
316 treatment strategies using longstanding p38 $\alpha$  inhibition should consider the potential  
317 cardiovascular risk among the possible secondary effects of the treatment.

318

bioRxiv preprint doi: <https://doi.org/10.1101/2021.11.15.468612>; this version posted November 16, 2021. The copyright holder for this preprint (which was not certified by peer review) is the author/funder, who has granted bioRxiv a license to display the preprint in perpetuity. It is made available under aCC-BY 4.0 International license.

## 319 MATERIALS AND METHODS

### 320 Animal preparation

321 *Mkk3*<sup>-/-</sup> mice (B6.129-*Map2k3*<sup>tm1Flv</sup>) (Lu *et al.*, 1999; Wysk *et al.*, 1999) and *Mkk6*<sup>-/-</sup>  
322 mice (B6.129-*Map2k6*<sup>tm1Flv</sup>) (Brancho *et al.*, 2003) were as previously described. Mice  
323 with a germ-line mutation in the *Map2k6* gene and *LoxP* elements inserted into two  
324 introns (*Map2k6*<sup>LoxP</sup>) were generated as previously described<sup>24</sup>. To generate mice  
325 lacking MKK6 or p38δ in striated muscle, *Map2k6*<sup>LoxP</sup> or p38δ-negative (B6.129-  
326 *Mapk13tm1*) mice were crossed with the FVB-Tg(Ckmm-cre)5Khn/J line on the  
327 C57BL/6J background (Jackson Laboratory). Mice lacking MKK6 in cardiomyocytes  
328 were generated by crossing *Map2k6*<sup>LoxP</sup> mice with the Tg(Myh6-cre)2182Mds line on  
329 the C57BL/6J background (Jackson Laboratory). The p38γ-negative line (B6.129-  
330 *Mapk12tm1*) was crossed with the *Mkk6*<sup>-/-</sup> line (B6.129-*Map2k6*<sup>tm1Flv</sup>) to generate  
331 double knockout mice. Likewise, mice lacking p38δ in striated muscle were crossed  
332 with the *Mkk6*<sup>-/-</sup> (B6.129-*Map2k6*<sup>tm1Flv</sup>) line. Genotype was confirmed by PCR analysis  
333 of genomic DNA. For signaling studies, animals were killed by cervical dislocation. For  
334 rapamycin treatment, mice received daily intraperitoneal injections with rapamycin (LC  
335 Laboratories, R-5000) (2 mg kg<sup>-1</sup> per day) or vehicle (0.25 % polyethylene glycol  
336 (Sigma), 0.25 % Tween-20 (Sigma) in PBS); injections started at 4 weeks of age and  
337 continued until 9 weeks of age, when heart size was analyzed by echocardiography. All  
338 animal procedures conformed to EU Directive 86/609/EEC and Recommendation  
339 2007/526/EC regarding the protection of animals used for experimental and other  
340 scientific purposes, enacted under Spanish law 1201/2005.

341

### 342 Computed tomography scan

bioRxiv preprint doi: <https://doi.org/10.1101/2021.11.15.468612>; this version posted November 16, 2021. The copyright holder for this preprint (which was not certified by peer review) is the author/funder, who has granted bioRxiv a license to display the preprint in perpetuity. It is made available under a [CC-BY 4.0 International license](#).

343 Computed tomography (CT) studies were performed with a small-animal PET/CT  
344 scanner (nanoScan, Mediso, Hungary). For the acquisition, mice were anesthetized  
345 using isoflurane 2% and 1.8 L/min oxygen flow. Ophthalmic gel was placed in the eyes  
346 to prevent drying. CT was acquired using an X-ray beam current of 178  $\mu$ A and a tube  
347 voltage of 55 kVp with 360 projections of 500 ms in a helical scan with pitch 1 and  
348 binning 1:4. CT image was reconstructed using a Ramlack algorithm with a final  
349 resolution of 0.078 mm<sup>3</sup>.

350

### 351 **Histology**

352 Tissue samples were fixed in 10% formalin for 48 h, dehydrated, and embedded in  
353 paraffin. Sections (8  $\mu$ m) were cut and stained with hematoxylin and eosin (American  
354 Master Tech Scientific). Fibrosis was assessed by Picrosirius red staining (Sigma) and  
355 the positive area for fibrosis was quantified with Image J software (Schneider *et al*,  
356 2012). For wheat germ agglutinin (WGA) immunofluorescence, 8  $\mu$ m heart sections  
357 were prepared, washed in PBS, incubated for 2h in WGA-Alexa 488 lectin (Invitrogen,  
358 Carlsbad, CA, USA), and washed and mounted in anti-fade reagent. Four images ( $\times$ 20)  
359 were taken from each heart, and the areas of 100–200 cross-sectionally oriented  
360 cardiomyocytes were measured and analyzed with Image J software (Schneider *et al*,  
361 2012).

362

### 363 **Echocardiography**

364 Mice were anesthetized by inhalation of isoflurane and oxygen (1.25 % and 98.75 %,  
365 respectively), and echocardiography was performed with a 30-MHz transthoracic  
366 echocardiography probe. Images were obtained with the Vevo 2100 micro-ultrasound  
367 imaging system (VisualSonics, Toronto, Canada). Short-axis, long-axis, B-mode and

bioRxiv preprint doi: <https://doi.org/10.1101/2021.11.15.468612>; this version posted November 16, 2021. The copyright holder for this preprint (which was not certified by peer review) is the author/funder, who has granted bioRxiv a license to display the preprint in perpetuity. It is made available under aCC-BY 4.0 International license.

368 two-dimensional M-mode views were obtained. Scans were conducted by two  
369 experienced researchers blinded to the mouse genotype. Measurements of left  
370 parasternal long and short axes and M-mode images (left parasternal short axis) were  
371 obtained at a heart rate of 500–550 b.p.m. LV end-diastolic diameter (LVEDD), LV  
372 end-systolic diameter (LVESD), and wall thickness were measured from M-mode  
373 tracings, and the average of three consecutive cardiac cycles is reported. The LV  
374 fractional shortening percentage was calculated as  $([LVEDD-LVESD]/LVEDD) \times 100$ .  
375 MRI of lung was performed with a 7-T Agilent scanner (Agilent, Santa Clara, CA,  
376 USA) equipped with a DD2 console and an actively shielded gradient set (205/120  
377 insert of maximum 130 mT m<sup>-1</sup> gradient strength). To enhance the signal-to-noise ratio  
378 during image acquisition, we used a combination of a 72-mm inner diameter quadrature  
379 birdcage TX volume coil (Rapid Biomedical GmbH, Germany) and an actively  
380 detuning 30-mm flexible customized surface RX coil (Neos Biotec, Pamplona, Spain).  
381 After acquisition of a tripilot gradient-echo image, a gradient-echo sequence without  
382 gating was used to acquire oblique coronal slices (1-2 slices) and axial slices (7-10  
383 slices covering the entire lung, 72-s acquisition time per slice) using the following  
384 parameters: TR/TE=6.7/2.2 ms, flip angle=10 degree, bandwidth=100 kHz, field of  
385 view=3 × 3 cm, matrix=256 × 128, slice thickness=1 mm (ref. 40). These images were  
386 used to determine interventricular septum and left ventricle posterior wall thicknesses  
387 and left ventricle corrected mass; the short-axis M-mode quantification was chosen as  
388 the most representative. Function was estimated from the ejection fraction and  
389 fractional shortening obtained from M-mode views by a blinded echocardiography  
390 expert. For ejection fraction measurements, a long- or short-axis view of the heart was  
391 selected to obtain an M-mode registration in a line perpendicular to the left ventricular  
392 septum and posterior wall at the level of the mitral chordae tendineae.

393

### 394 **Immunoblot analysis**

395 Tissue extracts were prepared in Triton (20 mM Tris (pH 7.4), 1 % Triton X-100, 10 %  
396 glycerol, 137 mM NaCl, 2 mM EDTA, 25 mM  $\beta$ -glycerophosphate, 1 mM sodium  
397 orthovanadate, 1 mM phenylmethylsulfonyl fluoride, and 10  $\mu\text{g ml}^{-1}$  aprotinin and  
398 leupeptin). Extracts (20–50  $\mu\text{g}$  protein) and immunoprecipitates (prepared from 0.5-2  
399 mg) were examined by immunoblot. For immunoprecipitation assays, heart extracts  
400 were incubated with 1-4  $\mu\text{g}$  of a specific antibody coupled to protein-G-Sepharose.  
401 After incubation overnight at 4 °C with agitation, the captured proteins were centrifuged  
402 at 10,000g, the supernatants collected, and the beads washed four times in PBS1X.  
403 Beads were boiled for 5 min at 95 °C in 10  $\mu\text{l}$  sample buffer. Extracts and  
404 immunoprecipitates were examined by SDS–PAGE and blotted with antibodies to the  
405 following targets: p38 $\gamma$  and p38 $\delta$ (Sabio *et al*, 2005; Sabio *et al*, 2004) at 1  $\mu\text{g ml}^{-1}$ ;  
406 vinculin (Sigma); puromycin (Millipore clone 12D10); phospho-MKK3  
407 (Ser189)/MKK6 (Ser207), MKK3, MKK6, phospho-p38 MAPK (Thr180/Tyr182),  
408 phospho-mTOR (Ser2481), mTOR, phospho-p70S6 kinase (Thr 389) (108D2), p70S6  
409 kinase, phospho-S6 (Ser 235/236) (D57.2.2E), phospho-S6 (Ser 240/244) (61H9), S6  
410 ribosomal protein, phospho-FoxO1 (Thr24)/FoxO3a (Thr32), phospho-eEF2 (Thr56),  
411 phospho-eIF4G (Ser1108), phospho-eIF4B (Ser422), eIF4B, phospho-4EBP1  
412 (Thr37/46), and 4EBP1, all at a 1:1000 dilution. Immunocomplexes were detected by  
413 enhanced chemiluminescence (GE Healthcare Lifesciences).

414

### 415 ***In vivo* protein synthesis assay**

416 For all *in vivo* measurements of protein synthesis, mice were injected intraperitoneally  
417 with 0.040  $\mu\text{mol g}^{-1}$  puromycin dissolved in 100  $\mu\text{l}$  PBS. Exactly 30 min after injection,

bioRxiv preprint doi: <https://doi.org/10.1101/2021.11.15.468612>; this version posted November 16, 2021. The copyright holder for this preprint (which was not certified by peer review) is the author/funder, who has granted bioRxiv a license to display the preprint in perpetuity. It is made available under a [CC-BY 4.0 International license](#).

418 tissues were extracted and frozen in liquid N<sub>2</sub> for subsequent immunoblot analysis of  
 419 protein-incorporated puromycin.

420

#### 421 **Blood pressure and heart rate measurements**

422 Blood pressure and heart rate in mice was measured using the noninvasive tail-cuff  
 423 method(Kubota *et al*, 2006). The measures were performed in conscious mice placed in  
 424 a BP-2000 Blood Pressure Analysis System (Visitech Systems). 10 preliminary  
 425 measurements and 10 actual measurements were recorded and the average of the 10  
 426 actual measurements used for analysis. The animals were trained for 4 consecutive days  
 427 prior the actual measurements were registered. All the measurements were taken at the  
 428 same time of the day.

429

#### 430 **RT-qPCR**

431 RNA 500ng – extracted with RNAeasy Plus Mini kit (Qiagen) following manufacturer  
 432 instructions – was transcribed to cDNA, and RT-qPCR was performed using Fast Sybr  
 433 Green probe (Applied Biosystems) and the appropriate primers in the 7900 Fast Real  
 434 Time thermocycler (Applied Biosystems). Relative mRNA expression was normalized  
 435 to *Gapdh* mRNA measured in each sample. *Fnl* Fw: ATGTGGACCCCTCCTGATAGT,  
 436 Rev: GCCAGTGATTTTCAGCAAAGG; *Coll1a1* Fw: GTCCTCTTAGGGGCCACT,  
 437 Rev: CCACGTCTCACCATTGGGG; *Col3a1* Fw: CTGTAACATGGAAACTGGGGAAA,  
 438 Rev: CCATAGCTGAACTGAAAACCACC; *Nppa* Fw: GCTTCCAGGCCATATTGGAG,  
 439 Rev: GGGGGCATGACCTCATCTT; *Nppb* Fw: GAGGTCACCTATCCTCTGG, Rev:  
 440 GCCATTTCTCCGACTTTTCTC; *Acta-2* Fw: CCCAAAGCTAACCGGGAGAAG, Rev:  
 441 CCAGAATCCAACACGATGCC; *Myh7* Fw: ACTGTCAACACTAAGAGGGTCA, Rev:

bioRxiv preprint doi: <https://doi.org/10.1101/2021.11.15.468612>; this version posted November 16, 2021. The copyright holder for this preprint (which was not certified by peer review) is the author/funder, who has granted bioRxiv a license to display the preprint in perpetuity. It is made available under a [CC-BY 4.0 International license](#).

442 TTGGATGATTTGATCTTCCAGGG; *Gapdh* FW: TGAAGCAGGCATCTGAGGG, Rev:

443 CGAAGGTGGAAGAGTGGA

444

#### 445 **Statistical analysis**

446 Results are expressed as mean  $\pm$  SEM. A difference of  $P < 0.05$  was considered  
 447 significant. Gaussian (normal) distribution was determined using the Shapiro-Wilks  
 448 normality test. For normally distributed populations, differences between groups were  
 449 examined for statistical significance by two-tailed Student *t*-test (2 groups) and 1-way  
 450 ANOVA followed by Tukey post-test (3 or more groups). To test the respective roles of  
 451 treatment or age and genotype, a 2-way ANOVA was performed. Tukey or Sidak post-  
 452 test were subsequently employed when appropriate. For data that failed normality  
 453 testing, Mann-Whitney test (2 groups), or Kruskal-Wallis with Dunn post-test (3 or  
 454 more groups) was performed. Gehan-Breslow-Wilcoxon test was used to assess  
 455 significance in the Kaplan–Meier survival analysis.

456

#### 457 **ACKNOWLEDGEMENTS**

458 We thank S. Bartlett and F. Chanut for English editing. We are grateful to R.J. Davis,  
 459 A. Padmanabhan, M. Costa and C. López-Otín for critical reading of the manuscript.  
 460 We thank A. C. Silva (ana@anasilvaillustrations.com) for help with figure editing and  
 461 design. This work was funded by a CNIC Intramural Project Severo Ochoa (Expediente  
 462 12-2016 IGP) to GS and JJ and MINECO-FEDER, PID2019-104399RB-I00 to GS.  
 463 BGT was a fellow of FPI Severo Ochoa CNIC Program (SVP-2013-067639) and is an  
 464 American Heart Association Postdoctoral Fellow (18POST34080175). R.R.B is a  
 465 fellow of the FPU Program (FPU17/03847). The following grants provided additional  
 466 funding: GS is granted by funds from European Regional Development Fund (ERDF):

bioRxiv preprint doi: <https://doi.org/10.1101/2021.11.15.468612>; this version posted November 16, 2021. The copyright holder for this preprint (which was not certified by peer review) is the author/funder, who has granted bioRxiv a license to display the preprint in perpetuity. It is made available under a [CC-BY 4.0 International license](#).

467 EFSD/Lilly European Diabetes Research Programme Dr Sabio, Fundación AECC  
 468 PROYE19047SABI and Comunidad de Madrid IMMUNOTHERCAN-CM  
 469 B2017/BMD-3733; US National Heart, Lung, and Blood Institute (R01 Grant  
 470 HL122352), Fondos FEDER, Madrid, Spain, and Fundación Bancaria “La Caixa  
 471 (project HR19/52160013); Fundación La Marató TV3: Ayudas a la investigación en  
 472 enfermedades raras 2020 (LA MARATO-2020); and Instituto de Salud Carlos III to JJ.  
 473 IN. was funded by EFSD/Lilly grants (2017 and 2019), the CNIC IPP FP7 Marie Curie  
 474 Programme (PCOFUND-2012-600396), EFSD Rising Star award (2019), JDC-2018-  
 475 Incorporación (MIN/JDC1802). The CNIC is supported by the Instituto de Salud Carlos  
 476 III (ISCIII), the Ministerio de Ciencia e Innovación (MCIN) and the Pro CNIC  
 477 Foundation)

#### 478 **AUTHOR CONTRIBUTIONS**

479 G.S. conceived this project. B.G-T. and R.R-B. equally performed the primary  
 480 experiments, acquired, prepared figures, and analyzed the data. G.S., B.G-T. and R.R-B.  
 481 designed, developed the hypothesis and wrote the manuscript with input from all authors.  
 482 B.G-T., R.R-B. A.M., E.M., L.S., I.N., V.M-R., F.M.C.U., A.M.S., M.E.R., L.L-V.,  
 483 L.J.J-B, J.J., D.F-R. and V.B. help to perform some of the experiments and acquired  
 484 data and critically revised the manuscript. G.S. led and funded the project.

#### 485 **COMPETING INTEREST**

486 The authors declare that they have no competing interest.

#### 487 **REFERENCES**

488  
 489 Bernardo BC, Weeks KL, Pretorius L, McMullen JR (2010) Molecular distinction  
 490 between physiological and pathological cardiac hypertrophy: experimental findings and  
 491 therapeutic strategies. *Pharmacol Ther* 128: 191-227

bioRxiv preprint doi: <https://doi.org/10.1101/2021.11.15.468612>; this version posted November 16, 2021. The copyright holder for this preprint (which was not certified by peer review) is the author/funder, who has granted bioRxiv a license to display the preprint in perpetuity. It is made available under aCC-BY 4.0 International license.

- 492 Brancho D, Tanaka N, Jaeschke A, Ventura JJ, Keikar N, Tanaka Y, Kyuuma M,  
 493 Takeshita T, Flavell RA, Davis RJ (2003) Mechanism of p38 MAP kinase activation in  
 494 vivo. *Genes Dev* 17: 1969-1978
- 495 Braz JC, Bueno OF, Liang Q, Wilkins BJ, Dai YS, Parsons S, Braunwart J, Glascock  
 496 BJ, Klevitsky R, Kimball TF *et al* (2003) Targeted inhibition of p38 MAPK promotes  
 497 hypertrophic cardiomyopathy through upregulation of calcineurin-NFAT signaling. *J*  
 498 *Clin Invest* 111: 1475-1486
- 499 Bruning JC, Michael MD, Winnay JN, Hayashi T, Horsch D, Accili D, Goodyear LJ,  
 500 Kahn CR (1998) A muscle-specific insulin receptor knockout exhibits features of the  
 501 metabolic syndrome of NIDDM without altering glucose tolerance. *Mol Cell* 2: 559-569
- 502 Canovas B, Nebreda AR (2021) Diversity and versatility of p38 kinase signalling in  
 503 health and disease. *Nat Rev Mol Cell Biol* 22: 346-366
- 504 Condorelli G, Drusco A, Stassi G, Bellacosa A, Roncarati R, Iaccarino G, Russo MA,  
 505 Gu Y, Dalton N, Chung C *et al* (2002) Akt induces enhanced myocardial contractility  
 506 and cell size in vivo in transgenic mice. *Proc Natl Acad Sci U S A* 99: 12333-12338
- 507 del Barco Barrantes I, Coya JM, Maina F, Arthur JS, Nebreda AR (2011) Genetic  
 508 analysis of specific and redundant roles for p38alpha and p38beta MAPKs during  
 509 mouse development. *Proc Natl Acad Sci U S A* 108: 12764-12769
- 510 Delaughter MC, Taffet GE, Fiorotto ML, Entman ML, Schwartz RJ (1999) Local  
 511 insulin-like growth factor I expression induces physiologic, then pathologic, cardiac  
 512 hypertrophy in transgenic mice. *FASEB J* 13: 1923-1929
- 513 Gonzalez-Teran B, Lopez JA, Rodriguez E, Leiva L, Martinez-Martinez S, Bernal JA,  
 514 Jimenez-Borreguero LJ, Redondo JM, Vazquez J, Sabio G (2016) p38gamma and delta  
 515 promote heart hypertrophy by targeting the mTOR-inhibitory protein DEPTOR for  
 516 degradation. *Nat Commun* 7: 10477
- 517 Heineke J, Molkentin JD (2006) Regulation of cardiac hypertrophy by intracellular  
 518 signalling pathways. *Nat Rev Mol Cell Biol* 7: 589-600
- 519 Kang YJ (2006) Cardiac hypertrophy: a risk factor for QT-prolongation and cardiac  
 520 sudden death. *Toxicol Pathol* 34: 58-66
- 521 Kubota Y, Umegaki K, Kagota S, Tanaka N, Nakamura K, Kunitomo M, Shinozuka K  
 522 (2006) Evaluation of blood pressure measured by tail-cuff methods (without heating) in  
 523 spontaneously hypertensive rats. *Biol Pharm Bull* 29: 1756-1758
- 524 Lauschke J, Maisch B (2009) Athlete's heart or hypertrophic cardiomyopathy? *Clin Res*  
 525 *Cardiol* 98: 80-88
- 526 Lu HT, Yang DD, Wysk M, Gatti E, Mellman I, Davis RJ, Flavell RA (1999) Defective  
 527 IL-12 production in mitogen-activated protein (MAP) kinase kinase 3 (Mkk3)-deficient  
 528 mice. *Embo J* 18: 1845-1857
- 529 Maillet M, van Berlo JH, Molkentin JD (2013) Molecular basis of physiological heart  
 530 growth: fundamental concepts and new players. *Nat Rev Mol Cell Biol* 14: 38-48
- 531 Matesanz N, Bernardo E, Acin-Perez R, Manieri E, Perez-Sieira S, Hernandez-Cosido  
 532 L, Montalvo-Romeral V, Mora A, Rodriguez E, Leiva-Vega L *et al* (2017) MKK6  
 533 controls T3-mediated browning of white adipose tissue. *Nat Commun* 8: 856
- 534 Matesanz N, Nikolic I, Leiva M, Pulgarin-Alfaro M, Santamans AM, Bernardo E, Mora  
 535 A, Herrera-Melle L, Rodriguez E, Beiroa D *et al* (2018) p38alpha blocks brown adipose  
 536 tissue thermogenesis through p38delta inhibition. *PLoS Biol* 16: e2004455
- 537 Matsui T, Li L, Wu JC, Cook SA, Nagoshi T, Picard MH, Liao R, Rosenzweig A  
 538 (2002) Phenotypic spectrum caused by transgenic overexpression of activated Akt in the  
 539 heart. *J Biol Chem* 277: 22896-22901

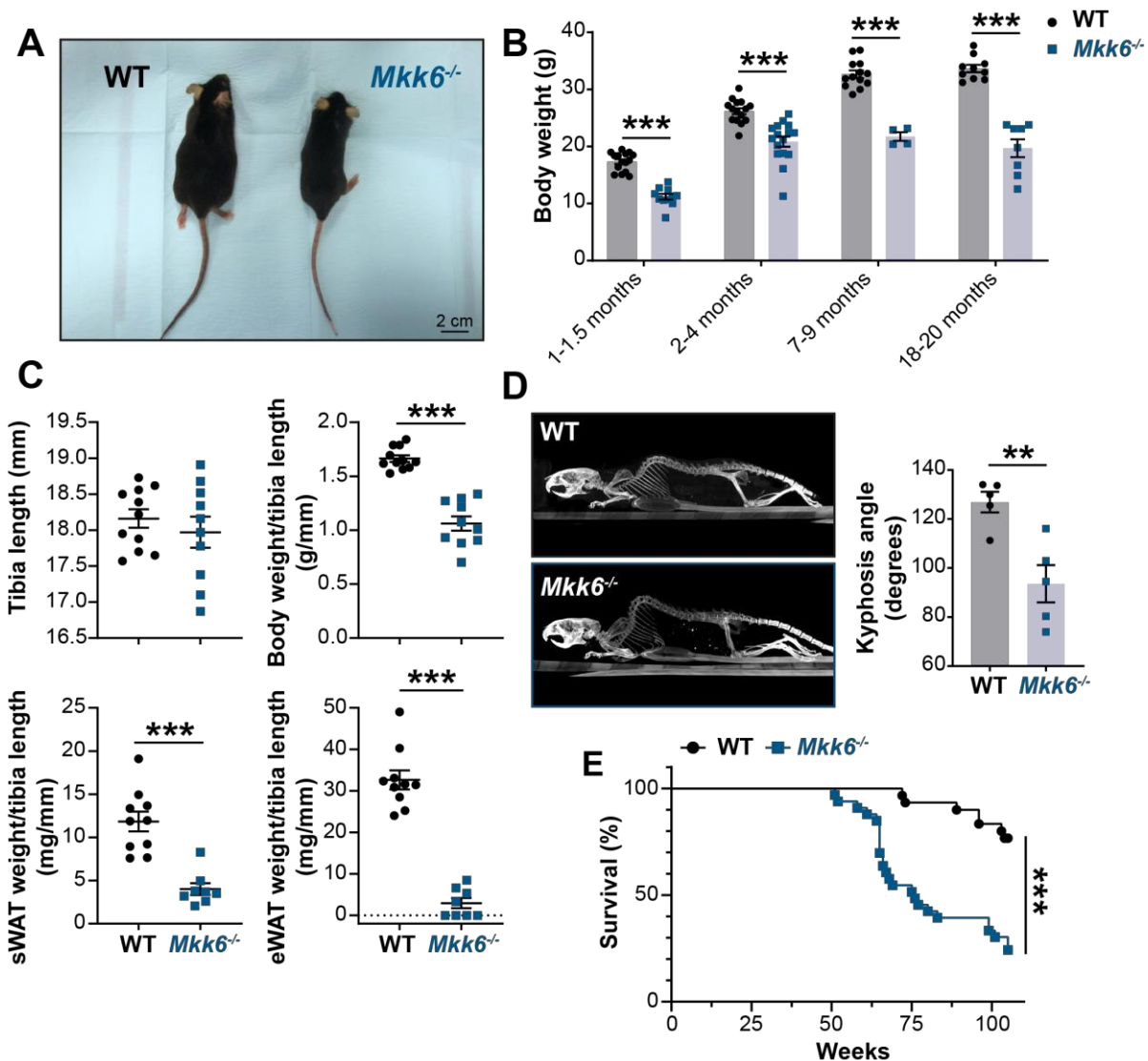
bioRxiv preprint doi: <https://doi.org/10.1101/2021.11.15.468612>; this version posted November 16, 2021. The copyright holder for this preprint (which was not certified by peer review) is the author/funder, who has granted bioRxiv a license to display the preprint in perpetuity. It is made available under aCC-BY 4.0 International license.

- 540 McFadden DG, Barbosa AC, Richardson JA, Schneider MD, Srivastava D, Olson EN  
 541 (2005) The Hand1 and Hand2 transcription factors regulate expansion of the embryonic  
 542 cardiac ventricles in a gene dosage-dependent manner. *Development* 132: 189-201
- 543 McMullen JR, Shioi T, Huang WY, Zhang L, Tarnavski O, Bisping E, Schinke M,  
 544 Kong S, Sherwood MC, Brown J *et al* (2004a) The insulin-like growth factor 1 receptor  
 545 induces physiological heart growth via the phosphoinositide 3-kinase(p110alpha)  
 546 pathway. *J Biol Chem* 279: 4782-4793
- 547 McMullen JR, Shioi T, Zhang L, Tarnavski O, Sherwood MC, Dorfman AL, Longnus  
 548 S, Pende M, Martin KA, Blenis J *et al* (2004b) Deletion of ribosomal S6 kinases does  
 549 not attenuate pathological, physiological, or insulin-like growth factor 1 receptor-  
 550 phosphoinositide 3-kinase-induced cardiac hypertrophy. *Mol Cell Biol* 24: 6231-6240
- 551 Nakamura M, Sadoshima J (2018) Mechanisms of physiological and pathological  
 552 cardiac hypertrophy. *Nat Rev Cardiol* 15: 387-407
- 553 Nikolic I, Leiva M, Sabio G (2020) The role of stress kinases in metabolic disease. *Nat*  
 554 *Rev Endocrinol*
- 555 Nishida K, Yamaguchi O, Hirotsu S, Hikoso S, Higuchi Y, Watanabe T, Takeda T,  
 556 Osuka S, Morita T, Kondoh G *et al* (2004) p38alpha mitogen-activated protein kinase  
 557 plays a critical role in cardiomyocyte survival but not in cardiac hypertrophic growth in  
 558 response to pressure overload. *Mol Cell Biol* 24: 10611-10620
- 559 Oldfield CJ, Duhamel TA, Dhalla NS (2020) Mechanisms for the transition from  
 560 physiological to pathological cardiac hypertrophy. *Can J Physiol Pharmacol* 98: 74-84
- 561 Porrello ER, Widdop RE, Delbridge LM (2008) Early origins of cardiac hypertrophy:  
 562 does cardiomyocyte attrition programme for pathological 'catch-up' growth of the heart?  
 563 *Clin Exp Pharmacol Physiol* 35: 1358-1364
- 564 Romero-Becerra R, Santamans AM, Folgueira C, Sabio G (2020) p38 MAPK Pathway  
 565 in the Heart: New Insights in Health and Disease. *Int J Mol Sci* 21
- 566 Sabio G, Arthur JS, Kuma Y, Peggie M, Carr J, Murray-Tait V, Centeno F, Goedert M,  
 567 Morrice NA, Cuenda A (2005) p38gamma regulates the localisation of SAP97 in the  
 568 cytoskeleton by modulating its interaction with GKAP. *Embo J* 24: 1134-1145
- 569 Sabio G, Reuver S, Feijoo C, Hasegawa M, Thomas GM, Centeno F, Kuhlendahl S,  
 570 Leal-Ortiz S, Goedert M, Garner C *et al* (2004) Stress- and mitogen-induced  
 571 phosphorylation of the synapse-associated protein SAP90/PSD-95 by activation of  
 572 SAPK3/p38gamma and ERK1/ERK2. *Biochem J* 380: 19-30
- 573 Schneider CA, Rasband WS, Eliceiri KW (2012) NIH Image to ImageJ: 25 years of  
 574 image analysis. *Nat Methods* 9: 671-675
- 575 Shimizu I, Minamino T (2016) Physiological and pathological cardiac hypertrophy. *J*  
 576 *Mol Cell Cardiol* 97: 245-262
- 577 Shioi T, Kang PM, Douglas PS, Hampe J, Yballe CM, Lawitts J, Cantley LC, Izumo S  
 578 (2000) The conserved phosphoinositide 3-kinase pathway determines heart size in mice.  
 579 *EMBO J* 19: 2537-2548
- 580 Shioi T, McMullen JR, Kang PM, Douglas PS, Obata T, Franke TF, Cantley LC, Izumo  
 581 S (2002) Akt/protein kinase B promotes organ growth in transgenic mice. *Mol Cell Biol*  
 582 22: 2799-2809
- 583 Shioi T, McMullen JR, Tarnavski O, Converso K, Sherwood MC, Manning WJ, Izumo  
 584 S (2003) Rapamycin attenuates load-induced cardiac hypertrophy in mice. *Circulation*  
 585 107: 1664-1670
- 586 Shiojima I, Sato K, Izumiya Y, Schiekofer S, Ito M, Liao R, Colucci WS, Walsh K  
 587 (2005) Disruption of coordinated cardiac hypertrophy and angiogenesis contributes to  
 588 the transition to heart failure. *J Clin Invest* 115: 2108-2118

bioRxiv preprint doi: <https://doi.org/10.1101/2021.11.15.468612>; this version posted November 16, 2021. The copyright holder for this preprint (which was not certified by peer review) is the author/funder, who has granted bioRxiv a license to display the preprint in perpetuity. It is made available under aCC-BY 4.0 International license.

589 Singhirunusorn P, Suzuki S, Kawasaki N, Saki I, Sakurai H (2005) Critical roles of  
590 threonine 187 phosphorylation in cellular stress-induced rapid and transient activation  
591 of transforming growth factor-beta-activated kinase 1 (TAK1) in a signaling complex  
592 containing TAK1-binding protein TAB1 and TAB2. *J Biol Chem* 280: 7359-7368  
593 Streicher JM, Ren S, Herschman H, Wang Y (2010) MAPK-activated protein kinase-2  
594 in cardiac hypertrophy and cyclooxygenase-2 regulation in heart. *Circ Res* 106: 1434-  
595 1443  
596 Tanaka N, Kamanaka M, Enslin H, Dong C, Wysk M, Davis RJ, Flavell RA (2002)  
597 Differential involvement of p38 mitogen-activated protein kinase kinases MKK3 and  
598 MKK6 in T-cell apoptosis. *EMBO Rep* 3: 785-791  
599 Wysk M, Yang DD, Lu HT, Flavell RA, Davis RJ (1999) Requirement of mitogen-  
600 activated protein kinase kinase 3 (MKK3) for tumor necrosis factor-induced cytokine  
601 expression. *Proc Natl Acad Sci U S A* 96: 3763-3768  
602 Zechner D, Thuerauf DJ, Hanford DS, McDonough PM, Glembotski CC (1997) A role  
603 for the p38 mitogen-activated protein kinase pathway in myocardial cell growth,  
604 sarcomeric organization, and cardiac-specific gene expression. *J Cell Biol* 139: 115-127  
605

bioRxiv preprint doi: <https://doi.org/10.1101/2021.11.15.468612>; this version posted November 16, 2021. The copyright holder for this preprint (which was not certified by peer review) is the author/funder, who has granted bioRxiv a license to display the preprint in perpetuity. It is made available under aCC-BY 4.0 International license.



606 **FIGURES**

607

608 **Figure 1. *Mkk6*<sup>-/-</sup> mice show a reduced survival age.** (A) Representative picture of 19-  
 609 month-old WT and *Mkk6*<sup>-/-</sup> male mice. Scale bar: 2 cm. (B) Body weight of WT ( $n=10-$   
 610 15) and *Mkk6*<sup>-/-</sup> ( $n=4-16$ ) mice over the indicated age period. 2-way ANOVA followed  
 611 by Sidak's post test. (C) Tibia length and body weight, subcutaneous white adipose  
 612 tissue (sWAT) and epididymal white adipose tissue (eWAT) to tibia length ratio from  
 613 20-month-old WT ( $n=10-11$ ) and *Mkk6*<sup>-/-</sup> ( $n=8-10$ ) mice. Unpaired *t*-test or Mann-  
 614 Whitney test. (D) Representative CT scan images and quantification of the column  
 615 kyphosis angle of 19-week-old WT ( $n=5$ ) and *Mkk6*<sup>-/-</sup> ( $n=5$ ) mice. Unpaired *t*-test. (E)

bioRxiv preprint doi: <https://doi.org/10.1101/2021.11.15.468612>; this version posted November 16, 2021. The copyright holder for this preprint (which was not certified by peer review) is the author/funder, who has granted bioRxiv a license to display the preprint in perpetuity. It is made available under a [CC-BY 4.0 International license](#).

616 Kaplan-Meier survival plot of age-related mortality in WT ( $n=30$ ) and *Mkk6*<sup>-/-</sup> ( $n=33$ )

617 mice. An endpoint of 105 weeks was chosen to avoid a severe worsening of the mice

618 health. Gehan-Breslow-Wilcoxon test. Data in B-D are mean  $\pm$  SEM. \*\* $P<0.01$ ;

619 \*\*\* $P<0.001$ .

bioRxiv preprint doi: <https://doi.org/10.1101/2021.11.15.468612>; this version posted November 16, 2021. The copyright holder for this preprint (which was not certified by peer review) is the author/funder, who has granted bioRxiv a license to display the preprint in perpetuity. It is made available under aCC-BY 4.0 International license.

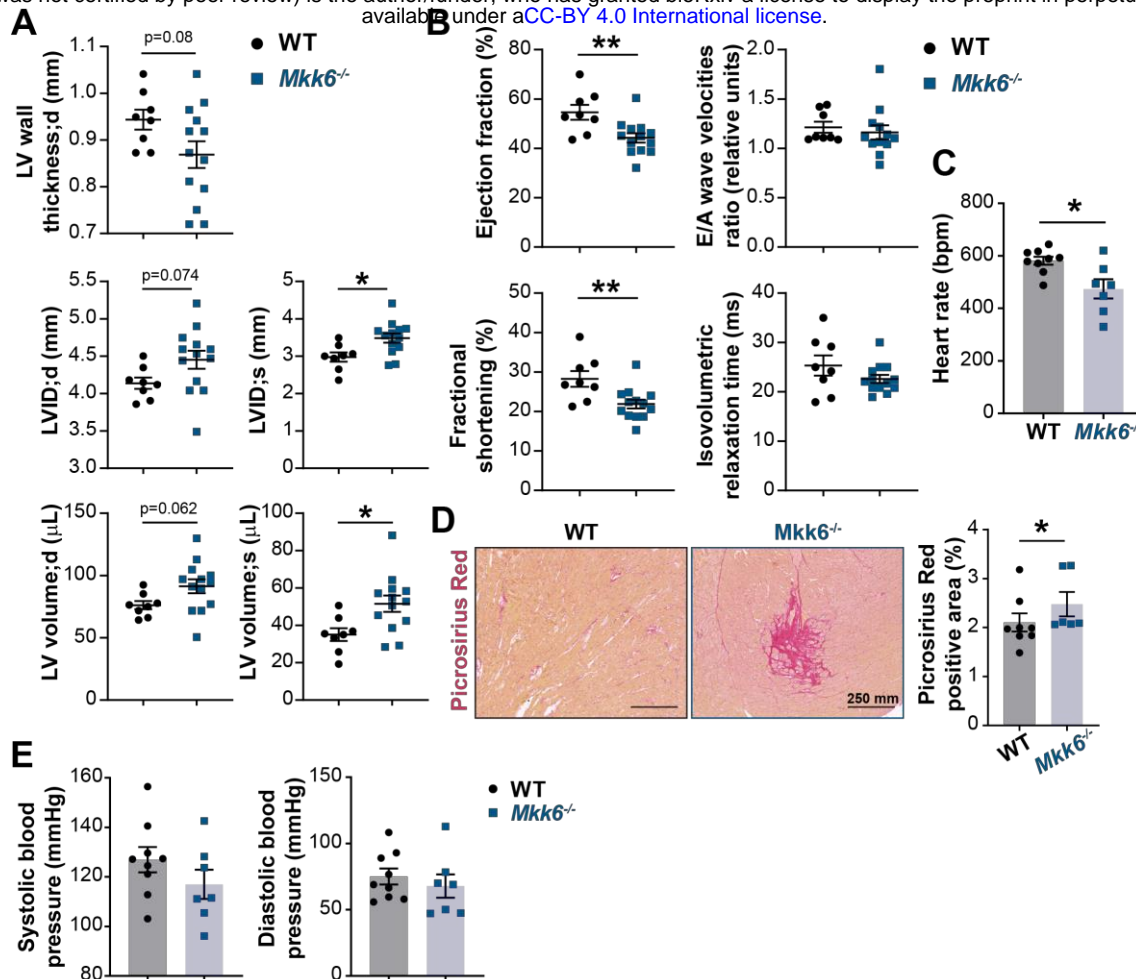
620 **Figure 1 – video supplement 1. Ataxia and hunched posture in *Mkk6*<sup>-/-</sup> mice.** Video

621 showing the movement of 18-month-old WT (left) and *Mkk6*<sup>-/-</sup> (right) mice. WT: wild

622 type.

623

bioRxiv preprint doi: <https://doi.org/10.1101/2021.11.15.468612>; this version posted November 16, 2021. The copyright holder for this preprint (which was not certified by peer review) is the author/funder, who has granted bioRxiv a license to display the preprint in perpetuity. It is made available under a [CC-BY 4.0 International license](#).



624

625 **Figure 2. MKK6 deficiency promotes cardiac dysfunction at advanced ages. (A, B)**

626 Echocardiography parameters related to left ventricle (LV) dimensions (A) and

627 contractility (B) in 12 to 14-month-old WT ( $n=8$ ) and *Mkk6*<sup>-/-</sup> ( $n=13$ ). Each dot

628 corresponds to an individual animal. LV wall thickness; d (left ventricle wall thickness

629 in diastole), LVID;d (left ventricular internal diameter in diastole), LVID;s (left

630 ventricular internal diameter in systole), LV volume;d (left ventricular volume in

631 diastole), LV volume;s (left ventricular volume in systole). Unpaired *t*-test. (C) Heart

632 rate in conscious 18-month-old WT ( $n=9$ ) and *Mkk6*<sup>-/-</sup> ( $n=7$ ) mice. bpm (beats per

633 minute). Unpaired *t*-test. (D) Picrosirius red staining and quantification of cardiac

634 fibrosis in 23 to 24-month-old WT ( $n=8$ ) and *Mkk6*<sup>-/-</sup> ( $n=6$ ) mice. Mann-Whitney test.

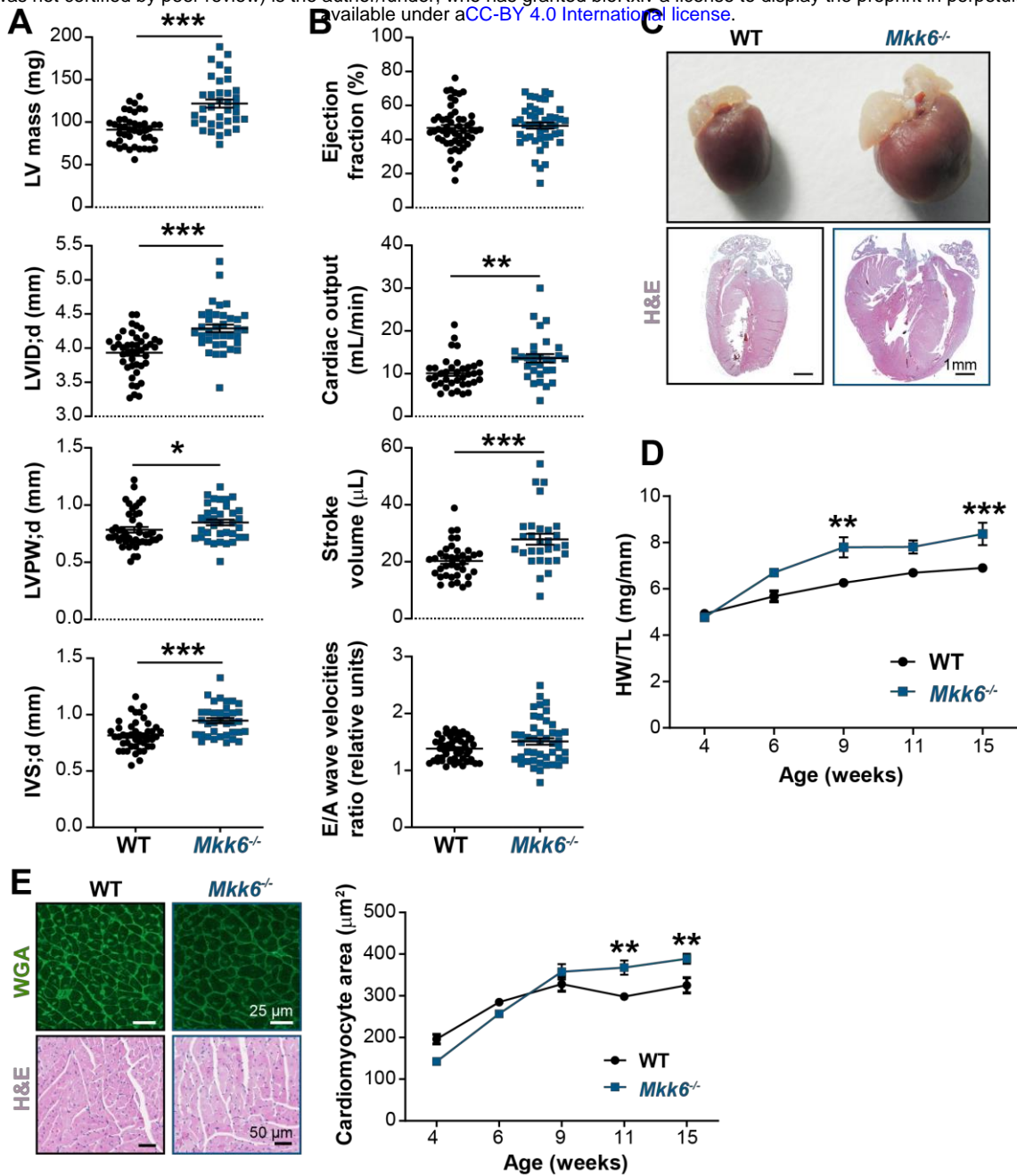
635 Scale bars: 250 μm. (E) Systolic and diastolic blood pressure in measured in conscious

bioRxiv preprint doi: <https://doi.org/10.1101/2021.11.15.468612>; this version posted November 16, 2021. The copyright holder for this preprint (which was not certified by peer review) is the author/funder, who has granted bioRxiv a license to display the preprint in perpetuity. It is made available under aCC-BY 4.0 International license.

636 18-month-old WT ( $n=9$ ) and  $Mkkb^{-/-}$  ( $n=7$ ) mice. Unpaired  $t$ -test. Data in A-E are mean

637  $\pm$  SEM. \* $P<0.05$ ; \*\* $P<0.01$ .

bioRxiv preprint doi: <https://doi.org/10.1101/2021.11.15.468612>; this version posted November 16, 2021. The copyright holder for this preprint (which was not certified by peer review) is the author/funder, who has granted bioRxiv a license to display the preprint in perpetuity. It is made available under aCC-BY 4.0 International license.



638

639 **Figure 3. Young MKK6-deficient hearts are hypertrophic with preserved cardiac**

640 **function.** (A, B) Echocardiography parameters related to left ventricle (LV) dimensions

641 (A) and contractility (B) in 9-week-old WT ( $n=37-54$ ) and *Mkk6*<sup>-/-</sup> ( $n=29-46$ ) mice.

642 Each dot corresponds to an individual mouse. Mean  $\pm$  SEM are shown as well. LV

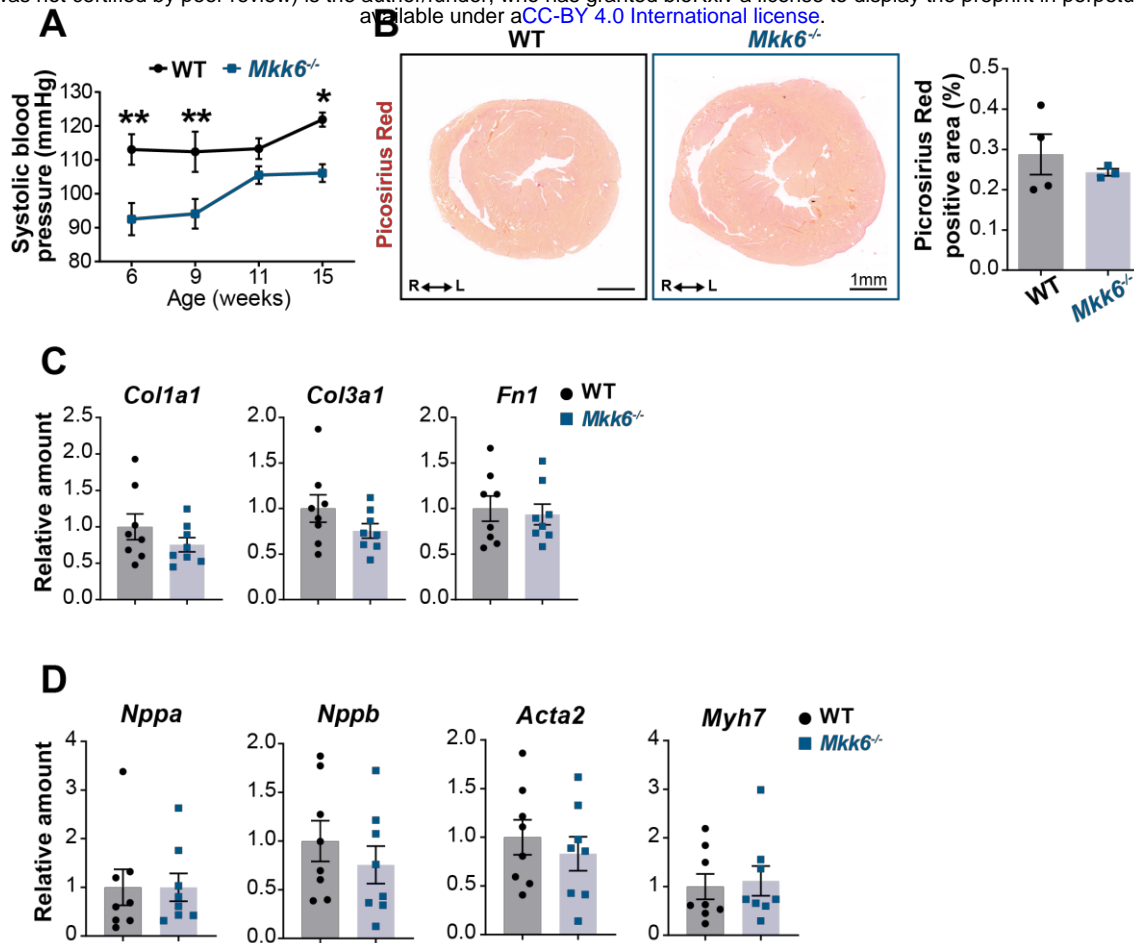
643 Mass (left ventricular mass), LVID;d (left ventricular internal diameter in diastole),

644 LVPW;d (left ventricular posterior wall in diastole), IVS;d (inter-ventricular septum in

bioRxiv preprint doi: <https://doi.org/10.1101/2021.11.15.468612>; this version posted November 16, 2021. The copyright holder for this preprint (which was not certified by peer review) is the author/funder, who has granted bioRxiv a license to display the preprint in perpetuity. It is made available under aCC-BY 4.0 International license.

645 diastole). Unpaired *t*-test or Mann-Whitney test. (C) Representative whole hearts and  
646 cardiac longitudinal sections stained with hematoxylin & eosin (H&E) from 9-week-old  
647 WT and *Mkk6*<sup>-/-</sup> mice. Scale bars: 1 mm. (D) Heart weight to tibia length ratio (HW/TL)  
648 of WT (*n*=4-15) and *Mkk6*<sup>-/-</sup> (*n*=5-14) over the indicated age period. 2-way ANOVA  
649 followed by Sidak's post test. (E) *Top*: Representative FITC wheat germ agglutinin  
650 (FITC-WGA)-stained heart sections from 9-week-old WT and *Mkk6*<sup>-/-</sup> mice and  
651 quantification of cardiomyocyte cross-sectional area over time (right graph, WT *n*=4-5;  
652 *Mkk6*<sup>-/-</sup> *n*=4-6, 2-way ANOVA followed by Sidak's post test). Scale bars: 25 μm.  
653 *Bottom*. Representative H&E-stained heart sections. Scale bars: 50 μm. Data in A, B, D  
654 and E are mean ± SEM. \**P*<0.05; \*\**P*<0.01; \*\*\**P*<0.001.

bioRxiv preprint doi: <https://doi.org/10.1101/2021.11.15.468612>; this version posted November 16, 2021. The copyright holder for this preprint (which was not certified by peer review) is the author/funder, who has granted bioRxiv a license to display the preprint in perpetuity. It is made available under aCC-BY 4.0 International license.



655

656

**Figure 3 – figure supplement 1. Evaluation of hallmarks of pathological cardiac**

657

**hypertrophy in young *Mkk6*<sup>-/-</sup> mice. (A)** Systolic blood pressure in WT (*n*=5) and

658

*Mkk6*<sup>-/-</sup> (*n*=4-7) mice at the indicated times after birth. 2-way ANOVA followed by

659

Sidak's post test. **(B)** Picosirius red staining and quantification of cardiac fibrosis in 9-

660

week-old WT (*n*=4) and *Mkk6*<sup>-/-</sup> (*n*=3) mice. Unpaired *t*-test. Scale bars: 1mm. **(C-D)**

661

Cardiac gene expression of fibrosis **(C)** and cardiac stress **(D)** markers in 9-week-old

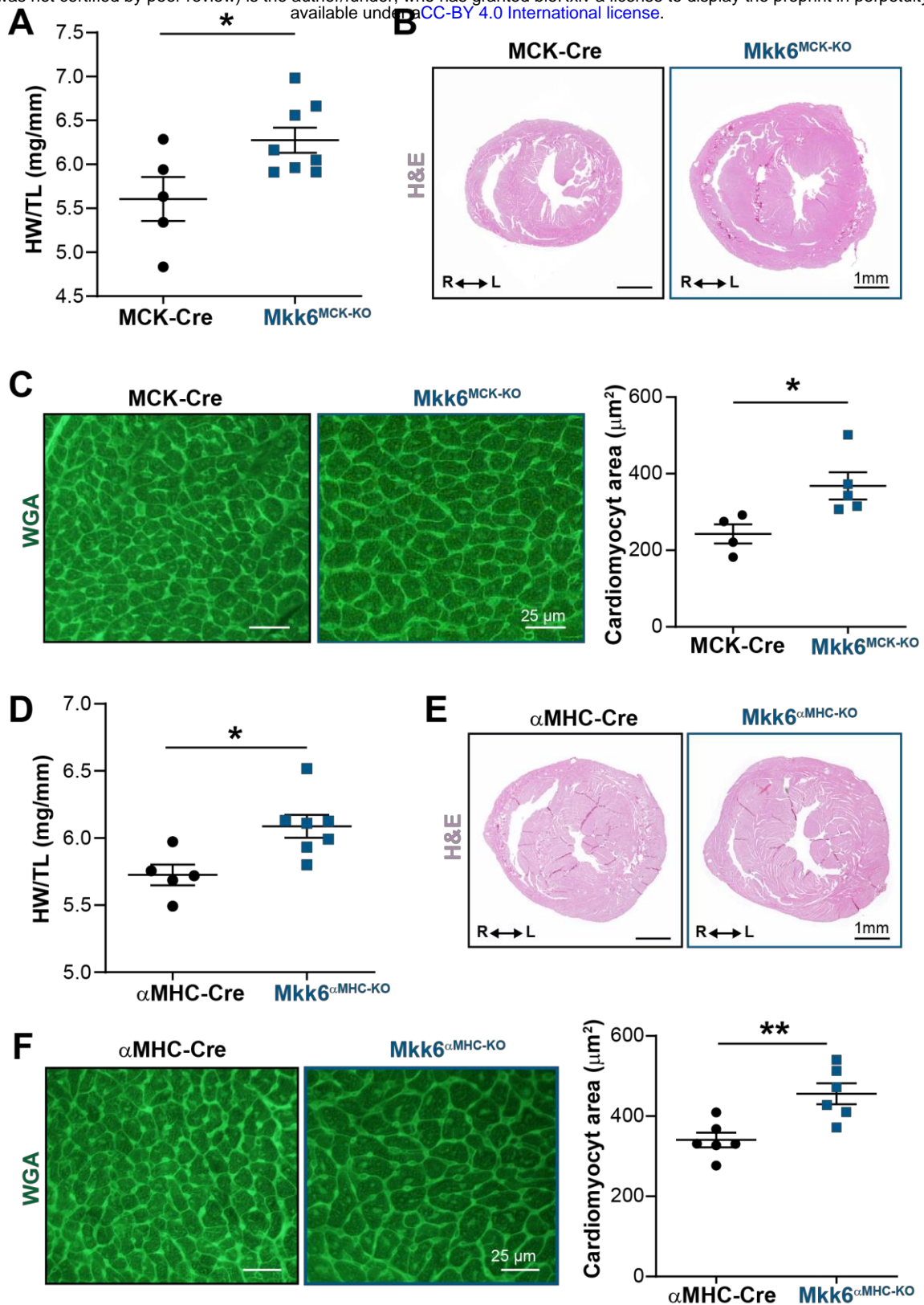
662

WT (*n*=8) and *Mkk6*<sup>-/-</sup> (*n*=8). Unpaired *t*-test or Mann-Whitney test. Data in A-D are

663

mean±SEM. \**P*<0.05. \*\**P*<0.001

bioRxiv preprint doi: <https://doi.org/10.1101/2021.11.15.468612>; this version posted November 16, 2021. The copyright holder for this preprint (which was not certified by peer review) is the author/funder, who has granted bioRxiv a license to display the preprint in perpetuity. It is made available under a [CC-BY 4.0 International license](https://creativecommons.org/licenses/by/4.0/).



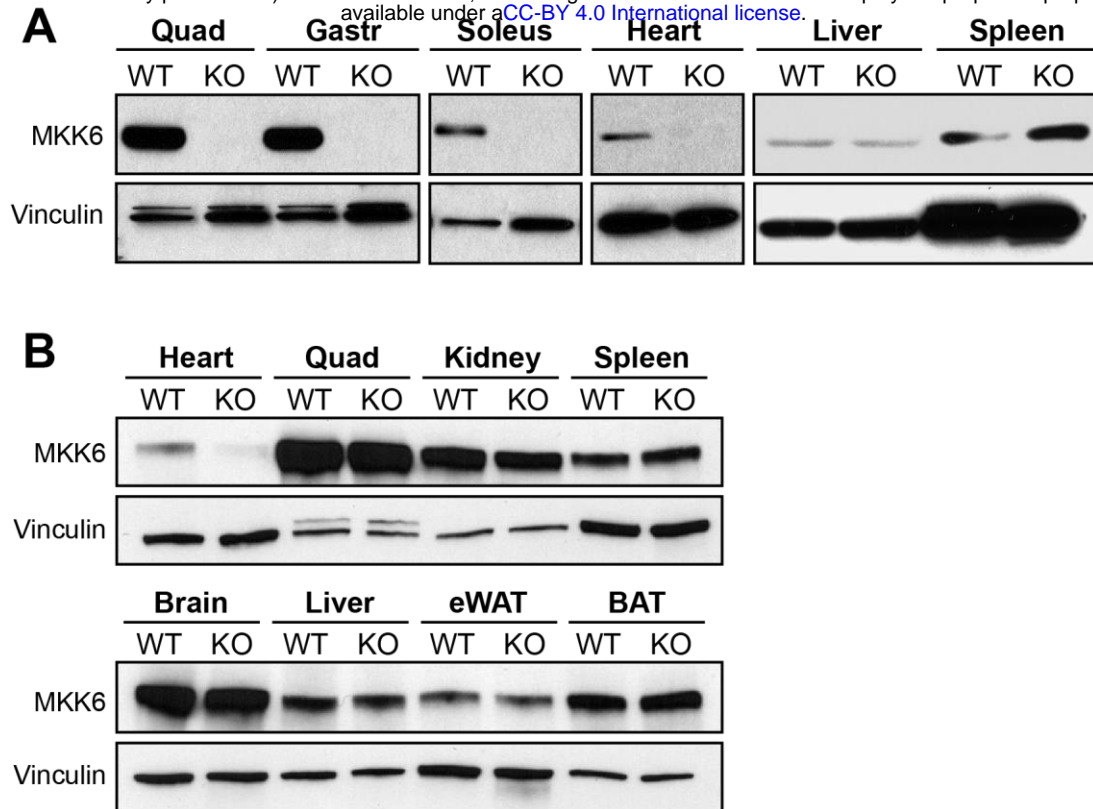
664

665 **Figure 4. Cardiac MKK6 controls postnatal heart growth.** (A) Heart weight to tibia  
 666 length ratio (HW/TL) in 9-week-old MCK-Cre (n=5) and *Mkk6*<sup>MCK-KO</sup> (n=8) mice.

bioRxiv preprint doi: <https://doi.org/10.1101/2021.11.15.468612>; this version posted November 16, 2021. The copyright holder for this preprint (which was not certified by peer review) is the author/funder, who has granted bioRxiv a license to display the preprint in perpetuity. It is made available under a [CC-BY 4.0 International license](#).

667 Unpaired *t*-test. **(B)** H&E-stained transverse cardiac sections from control (MCK-Cre)  
668 and Mkk6<sup>MCK-KO</sup> mice. Scale bars: 1 mm. **(C)** Representative FITC wheat germ  
669 agglutinin (FITC-WGA) staining and corresponding quantification of cardiomyocyte  
670 cross-sectional area in MCK-Cre (*n*=4) and Mkk6<sup>MCK-KO</sup> (*n*=5) mice. Unpaired *t*-test.  
671 Scale bars: 25 μm. **(D)** Heart weight to tibia length ratio in 9-week-old αMHC-Cre  
672 (*n*=5) and MKK6<sup>αMHC-KO</sup> (*n*=7) mice. Unpaired *t*-test. **(E)** H&E-stained transverse heart  
673 sections from αMHC-Cre and MKK6<sup>αMHC-KO</sup> mice. Scale bars: 1 mm. **(F)**  
674 Representative FITC-WGA staining and corresponding quantification of cardiomyocyte  
675 cross-sectional area in αMHC-Cre (*n*=6) and MKK6<sup>αMHC-KO</sup> (*n*=6) mice. Unpaired *t*-  
676 test. Scale bars: 25 μm. Data in A, C, D and F are mean ± SEM. \**P*<0.05; \*\**P*<0.01.

bioRxiv preprint doi: <https://doi.org/10.1101/2021.11.15.468612>; this version posted November 16, 2021. The copyright holder for this preprint (which was not certified by peer review) is the author/funder, who has granted bioRxiv a license to display the preprint in perpetuity. It is made available under a [CC-BY 4.0 International license](#).

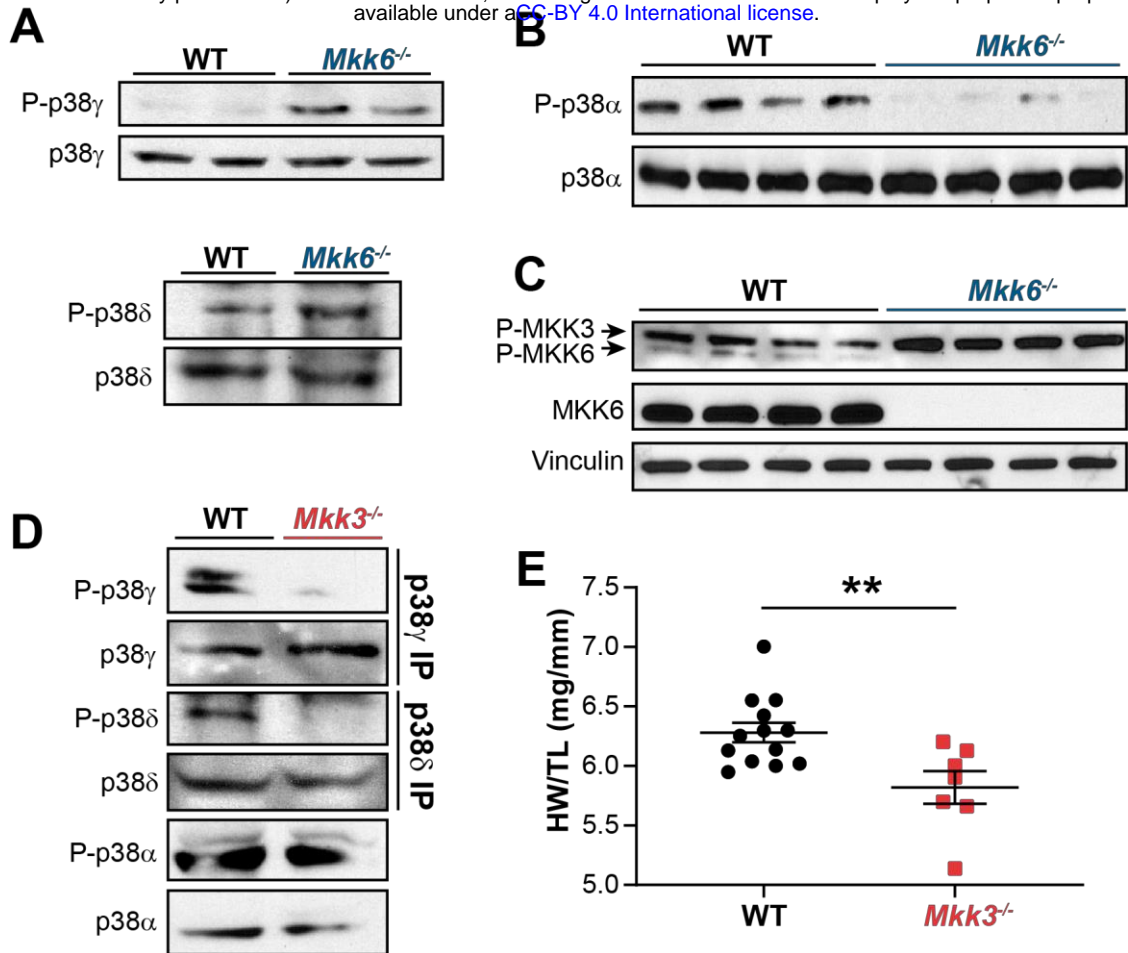


677

678

679 **Figure 4 – figure supplement 1. Tissue-specific MKK6 deletion in  $Mkk6^{MCK-KO}$  and**  
 680  **$Mkk6^{\alpha MHC-KO}$  mice. (A) Confirmation of MKK6 deletion in tissue lysates from**  
 681  **$Mkk6^{MCK-KO}$  (KO) mice in quadriceps (Quad), gastronemius (Gastr), soleus and heart,**  
 682 **but not in spleen and liver, and not in MCK-Cre (WT) tissues. (B) Confirmation of**  
 683 **specific MKK6 deletion in the heart of  $MKK6^{\alpha MHC-KO}$ , but not in lysates of  $\alpha MHC$ -Cre**  
 684 **(WT) and  $MKK6^{\alpha MHC-KO}$  (KO) quadriceps (Quad), kidney, spleen, brain, liver,**  
 685 **epididymal white adipose tissue (eWAT) and brown adipose tissue (BAT).**

bioRxiv preprint doi: <https://doi.org/10.1101/2021.11.15.468612>; this version posted November 16, 2021. The copyright holder for this preprint (which was not certified by peer review) is the author/funder, who has granted bioRxiv a license to display the preprint in perpetuity. It is made available under aCC-BY 4.0 International license.

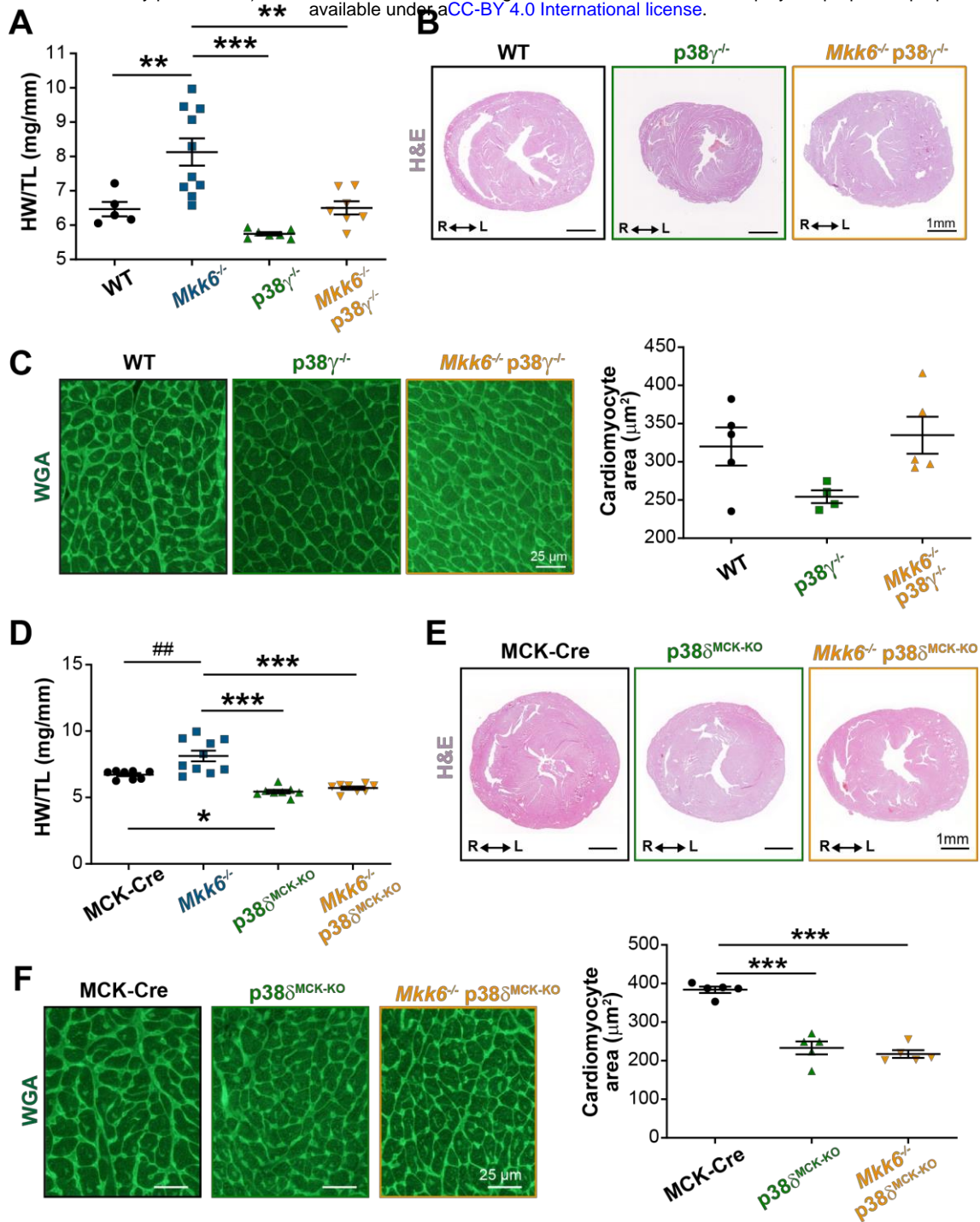


686

687 **Figure 5. MKK6 is necessary for p38 $\alpha$  phosphorylation and MKK3 for p38 $\gamma$  and**  
 688 **p38 $\delta$  phosphorylation in the heart. (A)** Western blot analysis of the phosphorylation  
 689 and amount of p38 $\gamma$  and  $\delta$  immunoprecipitated from heart lysates from 9-week-old WT  
 690 and *Mkk6*<sup>-/-</sup> mice. **(B)** Immunoblot analysis of p38 $\alpha$  phosphorylation and protein amount  
 691 in WT and *Mkk6*<sup>-/-</sup> mice. **(C)** Phosphorylation and protein levels of MKK3 and MKK6  
 692 in heart lysates from WT and *Mkk6*<sup>-/-</sup> mice. **(D)** Immunoprecipitation analysis of the  
 693 phosphorylation and protein amounts of p38 $\alpha$ , p38 $\gamma$  and p38 $\delta$  isoforms in heart lysates  
 694 from 9-week-old WT and *Mkk3*<sup>-/-</sup> mice. **(E)** Heart weight to tibia length ratio in WT  
 695 ( $n=13$ ) and *Mkk3*<sup>-/-</sup> ( $n=7$ ) mice at 9 weeks of age. Data in E are mean  $\pm$  SEM. ( $n=7-13$ ).  
 696 \*\* $P < 0.01$  (Unpaired  $t$ -test).

697

bioRxiv preprint doi: <https://doi.org/10.1101/2021.11.15.468612>; this version posted November 16, 2021. The copyright holder for this preprint (which was not certified by peer review) is the author/funder, who has granted bioRxiv a license to display the preprint in perpetuity. It is made available under aCC-BY 4.0 International license.



698

699 **Figure 6. Loss of p38 $\gamma/\delta$  in cardiomyocytes rescues the cardiac hypertrophy**

700 **induced by MKK6 deficiency.** All phenotypes shown come from 9-week-old mice.

701 (A) Heart weight to tibia length ratio in WT ( $n=5$ ), *Mkk6*<sup>-/-</sup> ( $n=10$ ), *p38*<sup>γ-/-</sup> ( $n=7$ ) and

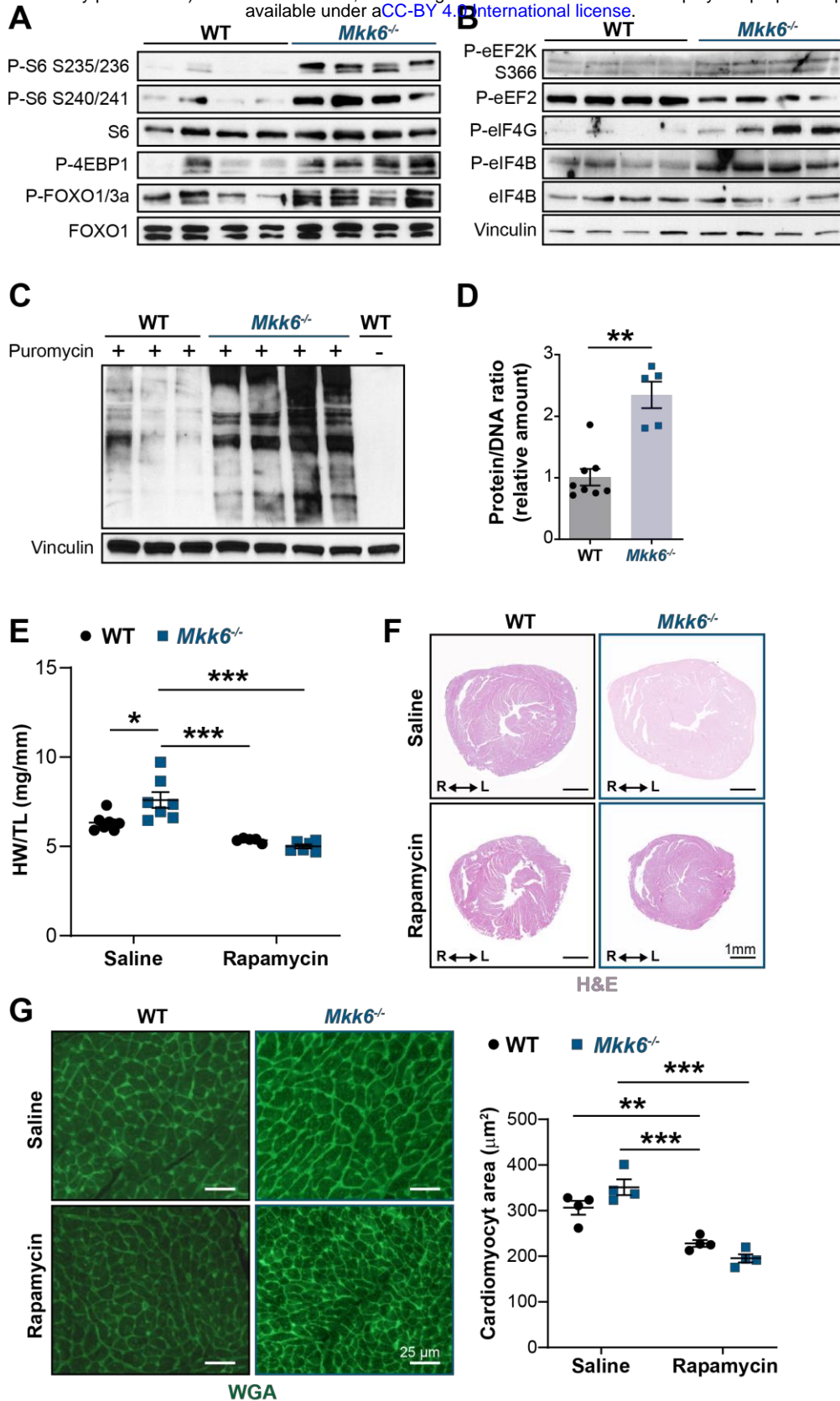
702 *Mkk6*<sup>-/-</sup> *p38*<sup>γ-/-</sup> ( $n=7$ ) mice. 1-way ANOVA followed by Tukey's post test. (B)

703 Representative H&E-stained transverse heart sections from WT, *p38*<sup>γ-/-</sup> and *Mkk6*<sup>-/-</sup>

bioRxiv preprint doi: <https://doi.org/10.1101/2021.11.15.468612>; this version posted November 16, 2021. The copyright holder for this preprint (which was not certified by peer review) is the author/funder, who has granted bioRxiv a license to display the preprint in perpetuity. It is made available under aCC-BY 4.0 International license.

704 p38 $\gamma^{-/-}$  mice. Scale bars: 1 mm. (C) Representative FITC-WGA staining and  
705 corresponding quantification of cardiomyocyte cross-sectional area in WT ( $n=5$ ), p38 $\gamma^{-/-}$   
706 ( $n=4$ ) and *Mkk6* $^{-/-}$  p38 $\gamma^{-/-}$  ( $n=5$ ) mice. Scale bars: 25  $\mu$ m. 1-way ANOVA followed by  
707 Tukey's post test. (D) Heart weight to tibia length ratio in MCK-Cre ( $n=8$ ), *Mkk6* $^{-/-}$   
708 ( $n=10$ ), p38 $\delta^{\text{MCK-KO}}$  ( $n=8$ ), and *Mkk6* $^{-/-}$  p38 $\delta^{\text{MCK-KO}}$  ( $n=8$ ) mice. Kruskal-Wallis test with  
709 Dunn's post-test (## $P<0.01$  Mann-Whitney test). (E) Representative H&E-stained  
710 transverse heart sections from MCK-Cre, p38 $\delta^{\text{MCK-KO}}$ , and *Mkk6* $^{-/-}$  p38 $\delta^{\text{MCK-KO}}$  mice.  
711 Scale bars: 1 mm. (F) Representative FITC-WGA staining and corresponding  
712 quantification of cardiomyocyte cross-sectional area in MCK-Cre ( $n=5$ ), p38 $\delta^{\text{MCK-KO}}$   
713 ( $n=5$ ), and *Mkk6* $^{-/-}$  p38 $\delta^{\text{MCK-KO}}$  ( $n=5$ ) mice. 1-way ANOVA followed by Tukey's post  
714 test. Scale bars: 25  $\mu$ m. The same data from *Mkk6* $^{-/-}$  mice was used in (A) and (D).  
715 Means  $\pm$  SEM are shown. \* $P<0.05$ ; \*\* $P<0.01$ ; \*\*\* $P<0.001$ ; ## $P<0.01$ .

bioRxiv preprint doi: <https://doi.org/10.1101/2021.11.15.468612>; this version posted November 16, 2021. The copyright holder for this preprint (which was not certified by peer review) is the author/funder, who has granted bioRxiv a license to display the preprint in perpetuity. It is made available under aCC-BY 4.0 International license.



716

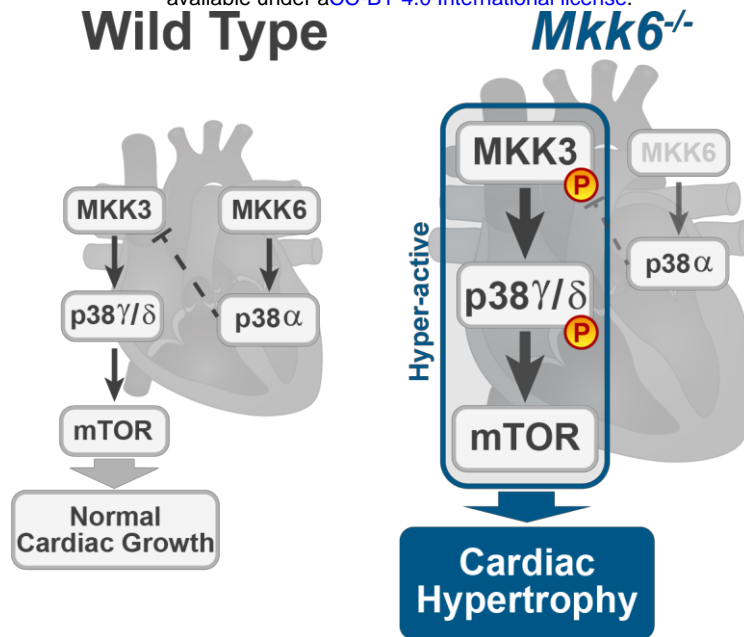
717 **Figure 7. Hyperactivation of mTOR signaling drives cardiac hypertrophy in *Mkk6***

718 ***-/-* mice. (A, B) Immunoblot analysis of mTOR signaling pathway activity (A) and**

bioRxiv preprint doi: <https://doi.org/10.1101/2021.11.15.468612>; this version posted November 16, 2021. The copyright holder for this preprint (which was not certified by peer review) is the author/funder, who has granted bioRxiv a license to display the preprint in perpetuity. It is made available under aCC-BY 4.0 International license.

719 activation status of translation factors **(B)** in heart lysates from 9-week-old WT and  
720 *Mkk6*<sup>-/-</sup> mice. **(C)** *In vivo* measurement of protein synthesis. Mice were injected  
721 intraperitoneally with 0.040 μmol g<sup>-1</sup> puromycin dissolved in 100 μl PBS. Exactly  
722 30 min after injection, tissues were extracted and frozen in liquid N<sub>2</sub> for immunoblot  
723 analysis with anti-puromycin antibody. **(D)** Protein content of WT (*n*=8) and *Mkk6*<sup>-/-</sup>  
724 (*n*=5) hearts measured as the protein-DNA ratio. Mann-Whitney test. **(E)** Heart weight  
725 to tibia length ratio in WT (*n*=5-7) and *Mkk6*<sup>-/-</sup> (*n*=6-7) mice after rapamycin treatment.  
726 Mice received daily intraperitoneal injections with rapamycin (2 mg kg<sup>-1</sup> per day) or  
727 vehicle from weeks 4 to 9 after birth. 2-way ANOVA followed by Tukey's posttest. **(F)**  
728 Representative H&E-stained transverse heart sections after treatment. Scale bars: 1 mm.  
729 **(G)** Representative FITC-WGA staining and corresponding quantification of  
730 cardiomyocyte cross-sectional area from WT (*n*=4) and *Mkk6*<sup>-/-</sup> (*n*=4) mice hearts after  
731 rapamycin treatment. 2-way ANOVA followed by Tukey's post test. Scale bars: 25 μm.  
732 Data in D, E and G are mean ± SEM. \**P*<0.05; \*\**P*<0.01; \*\*\**P*<0.001.

bioRxiv preprint doi: <https://doi.org/10.1101/2021.11.15.468612>; this version posted November 16, 2021. The copyright holder for this preprint (which was not certified by peer review) is the author/funder, who has granted bioRxiv a license to display the preprint in perpetuity. It is made available under aCC-BY 4.0 International license.



733

734 **Figure 8. Model for p38 $\gamma/\delta$  activation mediated cardiac hypertrophic growth.** In a  
 735 physiological context, MKK3-p38 $\gamma/\delta$  pathway promotes normal cardiac growth through  
 736 the activation of mTOR signaling pathway. MKK6 deficiency stimulates the  
 737 hyperactivation of MKK3-p38 $\gamma/\delta$  and the consequent increase in mTOR activity, which  
 738 drives increased cardiac hypertrophy.